

Pose Graph Optimization in the Complex Domain: Lagrangian Duality, Conditions For Zero Duality Gap, and Optimal Solutions

Giuseppe C. Calafiore*, Luca Carlone[†], and Frank Dellaert[‡]

Abstract

Pose Graph Optimization (PGO) is the problem of estimating a set of poses from pairwise relative measurements. PGO is a nonconvex problem, and currently no known technique can guarantee the computation of a global optimal solution. In this paper, we show that Lagrangian duality allows computing a globally optimal solution, under certain conditions that are satisfied in many practical cases. Our first contribution is to frame the PGO problem in the complex domain. This makes analysis easier and allows drawing connections with the recent literature on *unit gain graphs*. Exploiting this connection we prove nontrivial results about the spectrum of the matrix underlying the problem. The second contribution is to formulate and analyze the properties of the Lagrangian dual problem in the complex domain. The dual problem is a semidefinite program (SDP). Our analysis shows that the duality gap is connected to the number of eigenvalues of the *penalized pose graph matrix*, which arises from the solution of the SDP. We prove that if this matrix has a *single eigenvalue in zero*, then (i) the duality gap is zero, (ii) the primal PGO problem has a unique solution, and (iii) the primal solution can be computed by *scaling* an eigenvector of the penalized pose graph matrix. The third contribution is algorithmic: we exploit the dual problem and propose an algorithm that computes a guaranteed optimal solution for PGO when the penalized pose graph matrix satisfies the Single Zero Eigenvalue Property (SZEP). We also propose a variant that deals with the case in which

*G.C. Calafiore, Dipartimento di Automatica e Informatica, Politecnico di Torino, Italy. E-mail: giuseppe.calafiore@polito.it

[†]L. Carlone, School of Interactive Computing, College of Computing, Georgia Institute of Technology, Atlanta, GA, USA. E-mail: luca.carlone@gatech.edu

[‡]F. Dellaert, School of Interactive Computing, College of Computing, Georgia Institute of Technology, Atlanta, GA, USA. E-mail: dellaert@cc.gatech.edu

the SZEP is not satisfied. This variant, while possibly suboptimal, provides a very good estimate for PGO in practice. The fourth contribution is a numerical analysis. Empirical evidence shows that in the vast majority of cases (100% of the tests under noise regimes of practical robotics applications) the penalized pose graph matrix does satisfy the SZEP, hence our approach allows computing the global optimal solution. Finally, we report simple counterexamples in which the duality gap is nonzero, and discuss open problems.

1 Introduction

Pose graph optimization (PGO) consists in the estimation of the poses (positions and orientations) of a mobile robot, from relative pose measurements. The problem can be formulated as the minimization of a nonconvex cost, and can be conveniently visualized as a graph, in which a (to-be-estimated) pose is attached to each vertex, and a given relative pose measurement is associated to each edge.

PGO is a key problem in many application endeavours. In robotics, it lies at the core of state-of-the-art algorithms for localization and mapping in both single robot [53, 27, 34, 57, 37, 11, 26, 43, 12, 13] and multi robot [46, 1, 47, 48, 42] systems. In computer vision and control, problems that are closely related to PGO need to be solved for structure from motion [35, 55, 2, 36, 68, 38, 33], attitude synchronization [73, 39, 56], camera network calibration [77, 74], sensor network localization [59, 58], and distributed consensus on manifolds [64, 75]. Moreover, similar formulations arise in molecule structure determination from microscopy imaging [70, 3].

A motivating example in robotics is the one pictured in Fig. 1(a). A mobile robot is deployed in an unknown environment at time $t = 0$. The robot traverses the environment and at each discrete time step acquires a sensor measurement (e.g., distances from obstacles within the sensing radius). From wheel rotation, the robot is capable of measuring the relative motion between two consecutive poses (say, at time i and j). Moreover, comparing the sensor measurement, acquired at different times, the robot can also extrapolate relative measurements between non consecutive poses (e.g., between i and k in the figure). PGO uses these measurements to estimate robot poses. The graph underlying the problem is shown in Fig. 1(b), where we draw in different colors the edges due to relative motion measurements (the *odometric edges*, in black) and the edges connecting non-consecutive poses (the *loop closures*, in red). The importance of estimating the robot poses is two-fold. First, the knowledge of the current robot pose is often needed

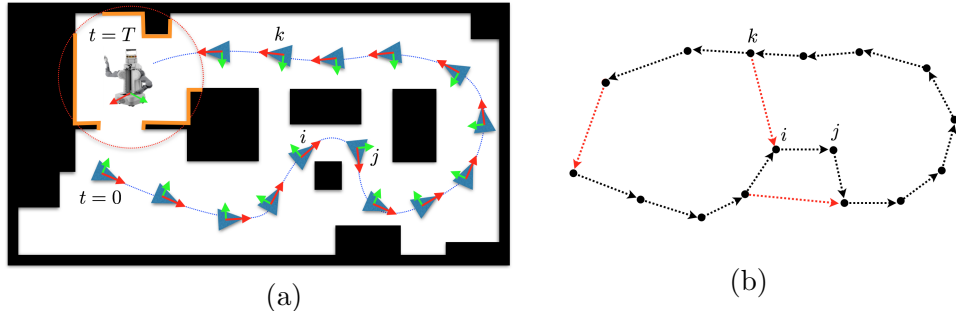


Figure 1: (a) Pose graph optimization in robotics. A mobile robot is deployed in an unknown environment at time $t = 0$. At each time step the robot measures distances from obstacles within the sensing radius (red circle). The sensor footprint (i.e., the set of measurements) at time T is visualized in orange. By matching sensor footprints acquired at different time steps, the robot establishes relative measurements between poses along its trajectory. PGO consists in the estimation of robot poses from these relative measurements. (b) Directed graph underlying the problem.

for performing high-level tasks within the environment. Second, from the knowledge of all past poses, the robot can *register* all sensor footprints in a common frame, and obtain a *map* of the environment, which is needed for model-based navigation and path planning.

Related work in robotics. Since the seminal paper [53], PGO attracted large attention from the robotics community. Most state-of-the-art techniques currently rely on iterative nonlinear optimization, which refines a given initial guess. The Gauss-Newton method is a popular choice [51, 45, 44], as it converges quickly when the initialization is close to a minimum of the cost function. Trust region methods (e.g., the Levenberg-Marquart method, or Powell’s Dog-Leg method [52]) have also been applied successfully to PGO [61, 62]; the gradient method has been shown to have a large convergence basin, while suffering from long convergence tails [57, 37, 48]. A large body of literature focuses on speeding up computation. This includes exploiting sparsity [45, 32], using reduction schemes to limit the number of poses [50, 9], faster linear solvers [34, 22], or approximate solutions [24, 12].

PGO is a nonconvex problem and iterative optimization techniques can only guarantee local convergence. State-of-the-art iterative solvers fail to converge to a global minimum of the cost for relatively small noise levels [13, 15]. This fact recently triggered efforts towards the design of more robust techniques, together with a theoretical analysis of PGO. Huang *et. al*

[41] discuss the number of local minima in small PGO problems. Knuth and Barooah [49] investigate the growth of the error in absence of loop closures. Carlone [10] provides conservative approximations of the basin of convergence for the Gauss-Newton method. Huang *et. al* [40] and Wang *et. al* [78] discuss the nonlinearities in PGO. In order to improve global convergence, a successful strategy consists in solving for the rotations first, and then using the resulting estimate to bootstrap iterative methods for PGO [11, 12, 13, 15]. This is convenient because the *rotation subproblem*¹ can be solved in closed-form in 2D [13], and many heuristic algorithms for rotation estimation also perform well in 3D [55, 35, 33, 15]. Despite the empirical success of state-of-the-art techniques, no approach can guarantee global convergence. It is not even known if the global optimizer itself is unique in general instances (while it is known that the minimizer is unique with probability one in the rotation subproblem [13]). The lack of guarantees promoted a recent interest in *verification* techniques for PGO. Carlone and Dellaert [14] use duality to evaluate the quality of a candidate solution in planar PGO. The work [14] also provides empirical evidence that in many problem instances the duality gap, i.e., the mismatch between the optimal cost of the primal and the dual problem, is zero.

Related work in other fields. Variations of the PGO problem appear in different research fields. In computer vision, a somehow more difficult variant of the problem is known as *bundle adjustment* [35, 55, 2, 36, 68, 38, 33]. Contrarily to PGO, in bundle adjustment the relative measurements between the (camera) poses are only known up to scale. While no closed-form solution is known for bundle adjustment, many authors focused on the solution of the rotation subproblem [35, 55, 2, 36, 68, 33, 38]. The corresponding algorithms have excellent performance in practice, but they come with little guarantees, as they are based on relaxation. Fredriksson and Olsson [33] use duality theory to design a verification technique for quaternion-based rotation estimation.

Related work in multi robot systems and sensor networks also includes contributions on rotation estimation (also known as *attitude synchronization* [73, 39, 56, 17, 79]). Borra *et. al* [6] propose a distributed algorithm for planar rotation estimation. Tron and Vidal [77, 74] provide convergence results for distributed attitude consensus using gradient descent; distributed consensus on manifold [64] is related to estimation from relative measure-

¹We use the term “rotation subproblem” to denote the problem of associating a rotation to each node in the graph, using relative rotation measurements. This corresponds to disregarding the translation measurements in PGO.

ments, as discussed in [75]. A problem that is formally equivalent to PGO is discussed in [59, 58] with application to sensor network localization. Pivovan *et. al* [59] provide observability conditions and discuss iterative algorithms that reduce the effect of noise. Peters *et. al* [58] study pose estimation in graphs with a single loop (related closed-form solutions also appear in other literatures [68, 25]), and provide an estimation algorithm over general graphs, based on the limit of a set of continuous-time differential equations, proving its effectiveness through numerical simulations. We only mention that a large literature in sensor network localization also deals with other types of relative measurements [54], including relative positions (with known rotations) [4, 63], relative distances [23, 30, 19, 5, 69, 8, 20, 21] and relative bearing measurements [72, 31, 76].

A less trivial connection can be established with related work in molecular structure determination from *cryo-electron microscopy* [70, 71], which offers very lucid and mature treatment of rotation estimation. Singer and Shkolnisky [70, 71] provide two approaches for rotation estimation, based on relaxation and semidefinite programming (SDP). Another merit of [70] is to draw connections between planar rotation estimation and the “MAX-2-LIN MOD L” problem in combinatorial optimization, and “MAX-K-CUT” problem in graph theory. Bandeira *et. al* [3] provide a Cheeger-like inequality that establishes performance bounds for the SDP relaxation. Saunderson *et. al* [66, 65] propose a tighter SDP relaxation, based on a spectrahedral representation of the convex hull of the rotation group.

Contribution. This paper shows that the use of Lagrangian duality allows computing a *guaranteed* globally optimal solution for PGO in many practical cases, and proves that in those cases the solution is unique.

Section 2 recalls preliminary concepts, and discusses the properties of a particular set of 2×2 matrices, which are scalar multiples of a planar rotation matrix. These matrices are omnipresent in planar PGO and acknowledging this fact allows reformulating the problem over complex variables.

Section 3 frames PGO as a problem in complex variables. This makes analysis easier and allows drawing connections with the recent literature on *unit gain graphs* [60]. Exploiting this connection we prove nontrivial results about the spectrum of the matrix underlying the problem (the *pose graph matrix*), such as the number of zero eigenvalues in particular graphs.

Section 4 formulates the Lagrangian dual problem in the complex domain. Moreover it presents an SDP relaxation of PGO, interpreting the relaxation as the dual of the dual problem. Our SDP relaxation is related to the one of [70, 33], but we deal with 2D poses, rather than rotations; moreover, we only use the SDP relaxation to complement our discussion on

duality and to support some of the proofs. Section 4.3 contains key results that relate the solution of the dual problem to the primal PGO problem. We show that the *duality gap* is connected to the zero eigenvalues of the *penalized pose graph matrix*, which arises from the solution of the dual problem. We prove that if this matrix has a *single eigenvalue in zero*, then (i) the duality gap is zero, (ii) the primal PGO problem has a unique solution (up to an arbitrary roto-translation), and (iii) the primal solution can be computed by *scaling* the eigenvector of the penalized pose graph matrix corresponding to the zero eigenvalue. To the best of our knowledge, this is the first work to discuss the uniqueness of the PGO solution for general graphs and to provide a provably optimal solution.

Section 5 exploits our analysis of the dual problem to devise computational approaches for PGO. We propose an algorithm that computes a guaranteed optimal solution for PGO when the penalized pose graph matrix satisfies the Single Zero Eigenvalue Property (SZEP). We also propose a variant that deals with the case in which the SZEP is not satisfied. This variant, while possibly suboptimal, is shown to perform well in practice, outperforming related approaches.

Section 6 elucidates on our theoretical results with numerical tests. In practical regimes of operation (rotation noise < 0.3 rad and translation noise < 0.5 m), our Monte Carlo runs always produced a penalized pose graph matrix satisfying the SZEP. Hence, in all tests with reasonable noise our approach enables the computation of the optimal solution. For larger noise levels (e.g., 1 rad standard deviation for rotation measurements), we observed cases in which the penalized pose graph matrix has multiple eigenvalues in zero. To stimulate further investigation towards structural results on duality (e.g., maximum level of noise for which the duality gap is provably zero) we report simple examples in which the duality gap is nonzero.

2 Notation and preliminary concepts

Section 2.1 introduces our notation. Section 2.2 recalls standard concepts from graph theory, and can be safely skipped by the expert reader. Section 2.3, instead, discusses the properties of the set of 2×2 matrices that are multiples of a planar rotation matrix. We denote this set with the symbol $\alpha SO(2)$. The set $\alpha SO(2)$ is of interest in this paper since the action of any matrix $Z \in \alpha SO(2)$ can be conveniently represented as a multiplication between complex numbers, as discussed in Section 3.3. Table 1 summarizes the main symbols used in this paper.

2.1 Notation

The cardinality of a set \mathcal{V} is written as $|\mathcal{V}|$. The sets of real and complex numbers are denoted with \mathbb{R} and \mathbb{C} , respectively. I_n denotes the $n \times n$ identity matrix, $\mathbf{1}_n$ denotes the (column) vector of all ones of dimension n , $0_{n \times m}$ denotes the $n \times m$ matrix of all zeros (we also use the shorthand $0_n \doteq 0_{n \times 1}$). For a matrix M , M_{ij} denotes the element of M in row i and column j . For matrices with a block structure we use $[M]_{ij}$ to denote the $d \times d$ block of M at the block row i and block column j . In this paper we only deal with matrices that have 2×2 blocks, i.e., $d = 2$, hence the notation $[M]_{ij}$ is unambiguous.

2.2 Graph terminology

A *directed graph* \mathcal{G} is a pair $(\mathcal{V}, \mathcal{E})$, where the *vertices* or *nodes* \mathcal{V} are a finite set of elements, and $\mathcal{E} \subset \mathcal{V} \times \mathcal{V}$ is the set of *edges*. Each edge is an ordered pair $e = (i, j)$. We say that e is *incident* on nodes i and j , *leaves* node i , called *tail*, and is *directed towards* node j , called *head*. The number of nodes is denoted with $n \doteq |\mathcal{V}|$, while the number of edges is $m \doteq |\mathcal{E}|$.

The *incidence matrix* \mathcal{A} of a directed graph is a $m \times n$ matrix with elements in $\{-1, 0, +1\}$ that exhaustively describes the graph topology. Each row of \mathcal{A} corresponds to an edge and has exactly two non-zero elements. For the row corresponding to edge $e = (i, j)$, there is a -1 on the i -th column and a $+1$ on the j -th column.

The set of *outgoing neighbors* of node i is $\mathcal{N}_i^{\text{out}} \doteq \{j : (i, j) \in \mathcal{E}\}$. The set of *incoming neighbors* of node i is $\mathcal{N}_i^{\text{in}} \doteq \{j : (j, i) \in \mathcal{E}\}$. The set of *neighbors* of node i is the union of outgoing and incoming neighbors $\mathcal{N}_i \doteq \mathcal{N}_i^{\text{out}} \cup \mathcal{N}_i^{\text{in}}$.

2.3 The set $\alpha SO(2)$

The set $\alpha SO(2)$ is defined as

$$\alpha SO(2) \doteq \{\alpha R : \alpha \in \mathbb{R}, R \in SO(2)\},$$

where $SO(2)$ is the set of 2D rotation matrices. Recall that $SO(2)$ can be parametrized by an angle $\theta \in (-\pi, +\pi]$, and any matrix $R \in SO(2)$ is in the form:

$$R = R(\theta) = \begin{bmatrix} \cos(\theta) & -\sin(\theta) \\ \sin(\theta) & \cos(\theta) \end{bmatrix}. \quad (1)$$

Clearly, $SO(2) \subset \alpha SO(2)$. The set $\alpha SO(2)$ is closed under standard matrix *multiplication*, i.e., for any $Z_1, Z_2 \in \alpha SO(2)$, also the product $Z_1 Z_2 \in$

$\alpha SO(2)$. In full analogy with $SO(2)$, it is also trivial to show that the multiplication is commutative, i.e., for any $Z_1, Z_2 \in \alpha SO(2)$ it holds that $Z_1 Z_2 = Z_2 Z_1$. Moreover, for $Z = \alpha R$ with $R \in SO(2)$ it holds that $Z^\top Z = |\alpha|^2 I_2$. The set $\alpha SO(2)$ is also closed under matrix *addition*, since for $R_1, R_2 \in SO(2)$, we have that

$$\begin{aligned} \alpha_1 R_1 + \alpha_2 R_2 &= \alpha_1 \begin{bmatrix} c_1 & -s_1 \\ s_1 & c_1 \end{bmatrix} + \alpha_2 \begin{bmatrix} c_2 & -s_2 \\ s_2 & c_2 \end{bmatrix} = \\ &= \begin{bmatrix} \alpha_1 c_1 + \alpha_2 c_2 & -(\alpha_1 s_1 + \alpha_2 s_2) \\ \alpha_1 s_1 + \alpha_2 s_2 & \alpha_1 c_1 + \alpha_2 c_2 \end{bmatrix} = \begin{bmatrix} a & -b \\ b & a \end{bmatrix} = \alpha_3 R_3, \end{aligned} \quad (2)$$

where we used the shorthands c_i and s_i for $\cos(\theta_i)$ and $\sin(\theta_i)$, and we defined $a \doteq \alpha_1 c_1 + \alpha_2 c_2$ and $b \doteq \alpha_1 s_1 + \alpha_2 s_2$. In (2), the scalar $\alpha_3 \doteq \pm\sqrt{a^2 + b^2}$ (if nonzero) normalizes $\begin{bmatrix} a & -b \\ b & a \end{bmatrix}$, such that $R_3 \doteq \begin{bmatrix} a/\alpha_3 & -b/\alpha_3 \\ b/\alpha_3 & a/\alpha_3 \end{bmatrix}$ is a rotation matrix; if $\alpha_3 = 0$, then $\alpha_1 R_1 + \alpha_2 R_2 = 0_{2 \times 2}$, which also falls in our definition of $\alpha SO(2)$. From this reasoning, it is clear that an alternative definition of $\alpha SO(2)$ is

$$\alpha SO(2) \doteq \left\{ \begin{bmatrix} a & -b \\ b & a \end{bmatrix} : a, b \in \mathbb{R} \right\}. \quad (3)$$

$\alpha SO(2)$ is tightly coupled with the set of complex numbers \mathbb{C} . Indeed, a matrix in the form (3) is also known as a *matrix representation* of a complex number [29]. We explore the implications of this fact for PGO in Section 3.3.

3 Pose graph optimization in the complex domain

3.1 Standard PGO

PGO estimates n poses from m relative pose measurements. We focus on the planar case, in which the i -th pose x_i is described by the pair $x_i \doteq (p_i, R_i)$, where $p_i \in \mathbb{R}^2$ is a position in the plane, and $R_i \in SO(2)$ is a planar rotation. The pose measurement between two nodes, say i and j , is described by the pair (Δ_{ij}, R_{ij}) , where $\Delta_{ij} \in \mathbb{R}^2$ and $R_{ij} \in SO(2)$ are the relative position and rotation measurements, respectively.

The problem can be visualized as a directed graph $\mathcal{G}(\mathcal{V}, \mathcal{E})$, where an unknown pose is attached to each node in the set \mathcal{V} , and each edge $(i, j) \in \mathcal{E}$ corresponds to a relative pose measurement between nodes i and j (Fig. 2).

In a noiseless case, the measurements satisfy:

$$\Delta_{ij} = R_i^\top (p_j - p_i), \quad R_{ij} = R_i^\top R_j, \quad (4)$$

Table 1: Symbols used in this paper

<i>Graph</i>	
$\mathcal{G} = (\mathcal{V}, \mathcal{E})$	Directed graph
m	Number of edges
n	Number of nodes
\mathcal{V}	Vertex set; $ \mathcal{V} = n$
\mathcal{E}	Edge set; $ \mathcal{E} = m$
$e = (i, j) \in \mathcal{E}$	Edge between nodes i and j
$\mathcal{A} \in \mathbb{R}^{n \times m}$	Incidence matrix of \mathcal{G}
$A \in \mathbb{R}^{(n-1) \times m}$	Anchored incidence matrix of \mathcal{G}
$\mathcal{L} = \mathcal{A}^\top \mathcal{A}$	Laplacian matrix of \mathcal{G}
$L = A^\top A$	Anchored Laplacian matrix of \mathcal{G}
<i>Real PGO formulation</i>	
$\bar{\mathcal{A}} = \mathcal{A} \otimes I_2$	Augmented incidence matrix
$\bar{A} = A \otimes I_2$	Augmented anchored incidence matrix
$\bar{\mathcal{L}} = \mathcal{L} \otimes I_2$	Augmented Laplacian matrix
$\mathcal{W} \in \mathbb{R}^{4n \times 4n}$	Real pose graph matrix
$W \in \mathbb{R}^{(4n-2) \times (4n-2)}$	Real anchored pose graph matrix
$p \in \mathbb{R}^{2n}$	Node positions
$\rho \in \mathbb{R}^{2(n-1)}$	Anchored node positions
$r \in \mathbb{R}^{2n}$	Node rotations
<i>Complex PGO formulation</i>	
$\tilde{W} \in \mathbb{C}^{(2n-1) \times (2n-1)}$	Complex anchored pose graph matrix
$\tilde{\rho} \in \mathbb{C}^{n-1}$	Anchored complex node positions
$\tilde{r} \in \mathbb{C}^n$	Complex node rotations
<i>Miscellanea</i>	
$SO(2)$	2D rotation matrices
$\alpha SO(2)$	Scalar multiple of a 2D rotation matrix
$ \mathcal{V} $	Cardinality of the set \mathcal{V}
I_n	$n \times n$ identity matrix
0_n (1_n)	Column vector of zeros (ones) of dimension n
$\text{Tr}(X)$	Trace of the matrix X

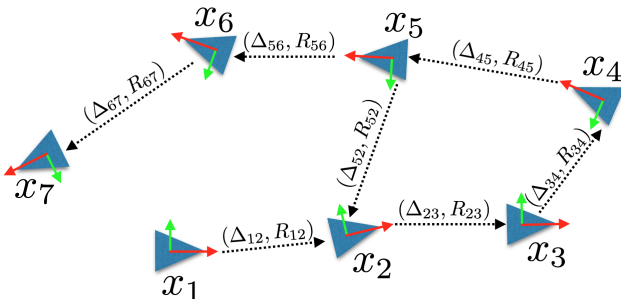


Figure 2: Schematic representation of Pose Graph Optimization: the objective is to associate a pose x_i to each node of a directed graph, given relative pose measurements (Δ_{ij}, R_{ij}) for each edge (i, j) in the graph.

and we can compute the unknown rotations $\{R_1, \dots, R_n\}$ and positions $\{p_1, \dots, p_n\}$ by solving a set of linear equations (relations (4) become linear after rearranging the rotation R_i to the left-hand side). In absence of noise, the problem admits a unique solution as long as one fixes the pose of a node (say $p_1 = 0_2$ and $R_1 = I_2$) and the underlying graph is connected.

In this work we focus on connected graphs, as these are the ones of practical interest in PGO (a graph with k connected components can be split in k subproblems, which can be solved and analyzed independently).

Assumption 1 (Connected Pose Graph) *The graph \mathcal{G} underlying the pose graph optimization problem is connected.*

In presence of noise, the relations (4) cannot be met exactly and pose graph optimization looks for a set of positions $\{p_1, \dots, p_n\}$ and rotations $\{R_1, \dots, R_n\}$ that minimize the mismatch with respect to the measurements. This mismatch can be quantified by different cost functions. We adopt the formulation proposed in [14]:

$$\min_{\{p_i\}, \{R_i\} \in SO(2)^n} \sum_{(i,j) \in \mathcal{E}} \|\Delta_{ij} - R_i^\top (p_j - p_i)\|_2^2 + \frac{1}{2} \|R_{ij} - R_i^\top R_j\|_F^2, \quad (5)$$

where $\|\cdot\|_2$ is the standard Euclidean distance and $\|\cdot\|_F$ is the Frobenius norm. The Frobenius norm $\|R_a - R_b\|$ is a standard measure of distance between two rotations R_a and R_b , and it is commonly referred to as the *chordal* distance, see, e.g., [38]. In (5), we used the short-hand notation $\{p_i\}$ (resp. $\{R_i\}$) to denote the set of unknown positions $\{p_1 \dots, p_n\}$ (resp. rotations).

Rearranging the terms, problem (5) can be rewritten as:

$$\min_{\{p_i\}, \{R_i\} \in SO(2)^n} \sum_{(i,j) \in \mathcal{E}} \|(p_j - p_i) - R_i \Delta_{ij}\|_2^2 + \frac{1}{2} \|R_j - R_i R_{ij}\|_F^2, \quad (6)$$

where we exploited the fact that the 2-norm is invariant to rotation, i.e., for any vector v and any rotation matrix R it holds $\|Rv\|_2 = \|v\|_2$. Eq. (6) highlights that the objective is a quadratic function of the unknowns.

The complexity of the problem stems from the fact that the constraint $R_i \in SO(2)$ is nonconvex, see, e.g., [65]. To make this more explicit, we follow the line of [14], and use a more convenient representation for nodes' rotations. Every planar rotation R_i can be written as in (1), and is fully defined by the vector

$$r_i = \begin{bmatrix} \cos(\theta_i) \\ \sin(\theta_i) \end{bmatrix}. \quad (7)$$

Using this parametrization and with simple matrix manipulation, Eq. (6) becomes (*cf.* with Eq. (11) in [14]):

$$\begin{aligned} \min_{\{p_i\}, \{r_i\}} \quad & \sum_{(i,j) \in \mathcal{E}} \|(p_j - p_i) - D_{ij} r_i\|_2^2 + \|r_j - R_{ij} r_i\|_2^2 \\ \text{s.t.} \quad & \|r_i\|_2^2 = 1, \quad i = 1, \dots, n \end{aligned} \quad (8)$$

where we defined:

$$D_{ij} = \begin{bmatrix} \Delta_{ij}^x & -\Delta_{ij}^y \\ \Delta_{ij}^y & \Delta_{ij}^x \end{bmatrix}, \quad (\text{with } \Delta_{ij} \doteq [\Delta_{ij}^x \ \Delta_{ij}^y]^\top), \quad (9)$$

and where the constraints $\|r_i\|_2^2 = 1$ specify that we look for vectors r_i that represent admissible rotations (i.e., such that $\cos(\theta_i)^2 + \sin(\theta_i)^2 = 1$).

Problem (8) is a quadratic problem with quadratic equality constraints. The latter are nonconvex, hence computing a local minimum of (8) is hard in general. There are two problem instances, however, for which it is easy to compute a global minimizer, which attains zero optimal cost. These two cases are recalled in Propositions 1-2.

Proposition 1 (Zero cost in trees) *An optimal solution for a PGO problem in the form (8) whose underlying graph is a tree attains zero cost.*

The proof is given in Appendix 8.1. Roughly speaking, in a tree, we can build an optimal solution by concatenating the relative pose measurements, and this solution annihilates the cost function. This comes with no surprises, as the *chords* (i.e., the extra edges, added to a spanning tree) are

indeed the elements that create redundancy and improve the pose estimate. However, also for graphs with chords, it is possible to attain the zero cost in problem (8).

Definition 1 (Balanced pose graph) *A pose graph is balanced if the pose measurements compose to the identity along each cycle in the graph²³.*

In a balanced pose graph, there exists a configuration that explains exactly the measurements, as formalized in the following proposition.

Proposition 2 (Zero cost in balanced pose graphs) *An optimal solution for a balanced pose graph optimization problem attains zero cost.*

The proof is given in Appendix 8.2. The concept of balanced graph describes a noiseless setup, while in real problem instances the measurements do not compose to the identity along cycles, because of the presence of noise.

We note the following fact, which will be useful in Section 3.2.

Proposition 3 (Coefficient matrices in PGO) *Matrices $D_{ij}, I_2, -I_2, R_{ij}$ appearing in (8) belong to $\alpha SO(2)$.*

This fact is trivial, since $R_{ij}, I_2 \in SO(2) \subset \alpha SO(2)$ (the latter also implies $-I_2 \in \alpha SO(2)$). Moreover, the structure of D_{ij} in (9) clearly falls in the definition of matrices in $\alpha SO(2)$ given in (3).

3.2 Matrix formulation and anchoring

In this section we rewrite the cost function (8) in a more convenient matrix form. The original cost is:

$$f(p, r) \doteq \sum_{(i,j) \in \mathcal{E}} \|(p_j - p_i) - D_{ij}r_i\|_2^2 + \|r_j - R_{ij}r_i\|_2^2 \quad (10)$$

where we denote with $p \in \mathbb{R}^{2n}$ and $r \in \mathbb{R}^{2n}$ the vectors stacking all nodes positions and rotations, respectively. Now, let $\mathcal{A} \in \mathbb{R}^{m \times n}$ denote the *incidence matrix* of the graph underlying the problem: if (i, j) is the k -th edge,

²We use the somehow standard term “composition” to denote the group operation for $SE(2)$. For two poses $T_1 \doteq (p_1, R_1)$ and $T_2 \doteq (p_2, R_2)$, the composition is $T_1 \cdot T_2 = (p_1 + R_1 p_2, R_1 R_2)$ [16]. Similarly, the *identity* element is $(0_2, I_2)$.

³When composing measurements along the loop, edge direction is important: for two consecutive edges (i, k) and (k, j) along the loop, the composition is $T_{ij} = T_{ik} \cdot T_{kj}$, while if the second edge is in the form (j, k) , the composition becomes $T_{ij} = T_{ik} \cdot T_{jk}^{-1}$.

then $\mathcal{A}_{ki} = -1$, $\mathcal{A}_{kj} = +1$. Let $\bar{\mathcal{A}} = \mathcal{A} \otimes I_2 \in \mathbb{R}^{2m \times 2n}$, and denote with $\bar{\mathcal{A}}_k \in \mathbb{R}^{2 \times 2n}$ the k -th block row of $\bar{\mathcal{A}}$. From the structure of $\bar{\mathcal{A}}$, it follows that $\bar{\mathcal{A}}_k p = p_j - p_i$. Also, we define $\bar{D} \in \mathbb{R}^{2m \times 2n}$ as a block matrix where the k -th block row $\bar{D}_k \in \mathbb{R}^{2 \times 2n}$ corresponding to the k -th edge (i, j) is all zeros, except for a 2×2 block $-D_{ij}$ in the i -th block column. Using the matrices $\bar{\mathcal{A}}$ and \bar{D} , the first sum in (10) can be written as:

$$\sum_{(i,j) \in \mathcal{E}} \|(p_j - p_i) - D_{ij} r_i\|_2^2 = \sum_{k=1}^m \|\bar{\mathcal{A}}_k p + \bar{D}_k r\|_2^2 = \|\bar{\mathcal{A}} p + \bar{D} r\|_2^2 \quad (11)$$

Similarly, we define $\bar{U} \in \mathbb{R}^{2m \times 2n}$ as a block matrix where the k -th block row $\bar{U}_k \in \mathbb{R}^{2 \times 2n}$ corresponding to the k -th edge (i, j) is all zeros, except for 2×2 blocks in the i -th and j -th block columns, which are equal to $-R_{ij}$ and I_2 , respectively. Using \bar{U} , the second sum in (10) becomes:

$$\sum_{(i,j) \in \mathcal{E}} \|r_j - R_{ij} r_i\|_2^2 = \sum_{k=1}^m \|\bar{U}_k r\|_2^2 = \|\bar{U} r\|_2^2 \quad (12)$$

Combining (11) and (12), the cost in (10) becomes:

$$\begin{aligned} f(p, r) &= \left\| \begin{bmatrix} \bar{\mathcal{A}} & \bar{D} \\ 0 & \bar{U} \end{bmatrix} \begin{bmatrix} p \\ r \end{bmatrix} \right\|_2^2 = \begin{bmatrix} p \\ r \end{bmatrix}^\top \begin{bmatrix} \bar{\mathcal{A}}^\top \bar{\mathcal{A}} & \bar{\mathcal{A}}^\top \bar{D} \\ \bar{D}^\top \bar{\mathcal{A}} & \bar{D}^\top \bar{D} + \bar{U}^\top \bar{U} \end{bmatrix} \begin{bmatrix} p \\ r \end{bmatrix} \\ &= \begin{bmatrix} p \\ r \end{bmatrix}^\top \begin{bmatrix} \bar{\mathcal{L}} & \bar{\mathcal{A}}^\top \bar{D} \\ \bar{D}^\top \bar{\mathcal{A}} & \bar{Q} \end{bmatrix} \begin{bmatrix} p \\ r \end{bmatrix}, \end{aligned} \quad (13)$$

where we defined $\bar{Q} \doteq \bar{D}^\top \bar{D} + \bar{U}^\top \bar{U}$ and $\bar{\mathcal{L}} \doteq \bar{\mathcal{A}}^\top \bar{\mathcal{A}}$, to simplify notation. Note that, since $\bar{\mathcal{A}} \doteq \mathcal{A} \otimes I_2$, it is easy to show that $\bar{\mathcal{L}} = \mathcal{L} \otimes I_2$, where $\mathcal{L} \doteq \mathcal{A}^\top \mathcal{A}$ is the Laplacian matrix of the graph underlying the problem. A pose graph optimization instance is thus completely defined by the matrix

$$\mathcal{W} \doteq \begin{bmatrix} \bar{\mathcal{L}} & \bar{\mathcal{A}}^\top \bar{D} \\ \bar{D}^\top \bar{\mathcal{A}} & \bar{Q} \end{bmatrix} \in \mathbb{R}^{4n \times 4n} \quad (14)$$

From (13), \mathcal{W} can be easily seen to be symmetric and positive semidefinite. Other useful properties of \mathcal{W} are stated in the next proposition.

Proposition 4 (Properties of \mathcal{W}) *Matrix \mathcal{W} in (14) is positive semidefinite, and*

1. *has at least two eigenvalues in zero;*

2. is composed by 2×2 blocks $[\mathcal{W}]_{ij}$, and each block is a multiple of a rotation matrix, i.e., $[\mathcal{W}]_{ij} \in \alpha SO(2)$, $\forall i, j = 1, \dots, 2n$. Moreover, the diagonal blocks of \mathcal{W} are nonnegative multiples of the identity matrix, i.e., $[\mathcal{W}]_{ii} = \alpha_{ii} I_2$, $\alpha_{ii} \geq 0$.

A formal proof of Proposition 4 is given in Appendix 8.3. An intuitive explanation of the second claim follows from the fact that (i) \mathcal{W} contains sums and products of the matrices in the original formulation (8) (which are in $\alpha SO(2)$ according to Lemma 3), and (ii) the set $\alpha SO(2)$ is closed under matrix sum and product (Section 2.3).

The presence of two eigenvalues in zero has a very natural geometric interpretation: the cost function encodes inter-nodal measurements, hence it is invariant to global translations of node positions, i.e., $f(p, r) = f(p + p_a, r)$, where $p_a \doteq (1_n \otimes I_2)a = [a^\top \dots a^\top]^\top$ (n copies of a), with $a \in \mathbb{R}^2$. Algebraically, this translates to the fact that the matrix $(1_n \otimes I_2) \in \mathbb{R}^{2n \times 2}$ is in the null space of the augmented incidence matrix \bar{A} , which also implies a two dimensional null space for \mathcal{W} .

Position anchoring In this paper we show that the duality properties in pose graph optimization are tightly coupled with the spectrum of the matrix \mathcal{W} . We are particularly interested in the eigenvalues at zero, and from this perspective it is not convenient to carry on the two null eigenvalues of \mathcal{W} (claim 1 of Proposition 4), which are always present, and are due to an intrinsic observability issue.

We remove the translation ambiguity by fixing the position of an arbitrary node. Without loss of generality, we fix the position p_1 of the first node to the origin, i.e., $p_1 = 0_2$. This process is commonly called *anchoring*. Setting $p_1 = 0$ is equivalent to removing the corresponding columns and rows from \mathcal{W} , leading to the following “anchored” PGO problem:

$$f(r, \rho) = \begin{bmatrix} 0_2 \\ \rho \\ r \end{bmatrix}^\top \mathcal{W} \begin{bmatrix} 0_2 \\ \rho \\ r \end{bmatrix} = \begin{bmatrix} \rho \\ r \end{bmatrix}^\top W \begin{bmatrix} \rho \\ r \end{bmatrix} \quad (15)$$

where ρ is the vector p without its first two-elements vector p_1 , and W is obtained from \mathcal{W} by removing the rows and the columns corresponding to p_1 . The structure of W is as follows:

$$W = \begin{bmatrix} \bar{A}^\top \bar{A} & \bar{A}^\top \bar{D} \\ \bar{D}^\top \bar{A} & \bar{Q} \end{bmatrix} \doteq \begin{bmatrix} \bar{L} & \bar{S} \\ \bar{S}^\top & \bar{Q} \end{bmatrix} \quad (16)$$

where $\bar{A} = A \otimes I_2$, and A is the *anchored* (or *reduced*) incidence matrix, obtained by removing the first column from \mathcal{A} , see, e.g., [12]. On the right-hand-side of (16) we defined $\bar{S} \doteq \bar{A}^\top \bar{D}$ and $\bar{L} \doteq \bar{A}^\top \bar{A}$.

We call W the *real (anchored) pose graph matrix*. W is still symmetric and positive semidefinite (it is a principal submatrix of a positive semidefinite matrix). Moreover, since W is obtained by removing a $2 \times 4n$ block row and a $4n \times 2$ block column from \mathcal{W} , it is still composed by 2×2 matrices in $\alpha SO(2)$, as specified in the following remark.

Remark 1 (Properties of W) *The positive semidefinite matrix W in (16) is composed by 2×2 blocks $[W]_{ij}$, that are such that $[W]_{ij} \in \alpha SO(2)$, $\forall i, j = 1, \dots, 2n - 1$. Moreover, the diagonal blocks of W are nonnegative multiples of the identity matrix, i.e., $[W]_{ii} = \alpha_{ii} I_2$, $\alpha \geq 0$.*

After anchoring, our PGO problem becomes:

$$\begin{aligned} f^* = \min_{\rho, r} & \begin{bmatrix} \rho \\ r \end{bmatrix}^\top W \begin{bmatrix} \rho \\ r \end{bmatrix} \\ \text{s.t.} & \|r_i\|_2^2 = 1, \quad i = 1, \dots, n \end{aligned} \quad (17)$$

3.3 To complex domain

In this section we reformulate problem (17), in which the decision variables are real vectors, into a problem in complex variables. The main motivation for this choice is that the real representation (17) is somehow redundant: as we will show in Proposition 7, each eigenvalue of W is repeated twice (multiplicity 2), while the complex representation does not have this redundancy, making analysis easier. In the rest of this paper, any quantity marked with a tilde ($\tilde{\cdot}$) lives in the complex domain \mathbb{C} .

Any real vector $v \in \mathbb{R}^2$ can be represented by a complex number $\tilde{v} = \eta e^{j\varphi}$, where $j^2 = -1$ is the *imaginary unit*, $\eta = \|v\|_2$ and φ is the angle that v forms with the horizontal axis. We use the operator $(\cdot)^\vee$ to map a 2-vector to the corresponding complex number, $\tilde{v} = v^\vee$. When convenient, we adopt the notation $v \sim \tilde{v}$, meaning that v and \tilde{v} are the vector and the complex representation of the same number.

The action of a real 2×2 matrix Z on a vector $v \in \mathbb{R}^2$ cannot be represented, in general, as a scalar multiplication between complex numbers. However, if $Z \in \alpha SO(2)$, this is possible. To show this, assume that $Z = \alpha R(\theta)$, where $R(\theta)$ is a counter-clockwise rotation of angle θ . Then,

$$Zv = \alpha R(\theta)v \sim \tilde{z} \tilde{v}, \quad \text{where } \tilde{z} = \alpha e^{j\theta}. \quad (18)$$

With slight abuse of notation we extend the operator $(\cdot)^\vee$ to $\alpha SO(2)$, such that, given $Z = \alpha R(\theta) \in \alpha SO(2)$, then $Z^\vee = \alpha e^{i\theta} \in \mathbb{C}$. By inspection, one can also verify the following relations between the sum and product of two matrices $Z_1, Z_2 \in \alpha SO(2)$ and their complex representations $Z_1^\vee, Z_2^\vee \in \mathbb{C}$:

$$(Z_1 Z_2)^\vee = \tilde{Z}_1^\vee Z_2^\vee \quad (Z_1 + Z_2)^\vee = Z_1^\vee + Z_2^\vee. \quad (19)$$

We next discuss how to apply the machinery introduced so far to reformulate problem (17) in the complex domain. The variables in problem (17) are the vectors $\rho \in \mathbb{R}^{2(n-1)}$ and $r \in \mathbb{R}^{2n}$ that are composed by 2-vectors, i.e., $\rho = [\rho_1^\top, \dots, \rho_{n-1}^\top]^\top$ and $r = [r_1^\top, \dots, r_n^\top]^\top$, where $\rho_i, r_i \in \mathbb{R}^2$. Therefore, we define the *complex positions* and the *complex rotations*:

$$\begin{aligned} \tilde{\rho} &= [\tilde{\rho}_1, \dots, \tilde{\rho}_{n-1}]^\top \in \mathbb{C}^{n-1}, & \text{where: } \tilde{\rho}_i &= \rho_i^\vee \\ \tilde{r} &= [\tilde{r}_1, \dots, \tilde{r}_n]^\top \in \mathbb{C}^n, & \text{where: } \tilde{r}_i &= r_i^\vee \end{aligned} \quad (20)$$

Using the complex parametrization (20), the constraints in (17) become:

$$|\tilde{r}_i|^2 = 1, \quad i = 1, \dots, n. \quad (21)$$

Similarly, we would like to rewrite the objective as a function of $\tilde{\rho}$ and \tilde{r} . This re-parametrization is formalized in the following proposition, whose proof is given in Appendix 8.4.

Proposition 5 (Cost in the complex domain) *For any pair (ρ, r) , the cost function in (17) is such that:*

$$f(\rho, r) = \begin{bmatrix} \rho \\ r \end{bmatrix}^\top W \begin{bmatrix} \rho \\ r \end{bmatrix} = \begin{bmatrix} \tilde{\rho} \\ \tilde{r} \end{bmatrix}^\top \tilde{W} \begin{bmatrix} \tilde{\rho} \\ \tilde{r} \end{bmatrix} \quad (22)$$

where the vectors $\tilde{\rho}$ and \tilde{r} are built from ρ and r as in (20), and the matrix $\tilde{W} \in \mathbb{C}^{(2n-1) \times (2n-1)}$ is such that $\tilde{W}_{ij} = [W]_{ij}^\vee$, with $i, j = 1, \dots, 2n-1$.

Remark 2 (Real diagonal entries for \tilde{W}) *According to Remark 1, the diagonal blocks of W are multiples of the identity matrix, i.e., $[W]_{ii} = \alpha_{ii} I_2$. Therefore, the diagonal elements of \tilde{W} are $\tilde{W}_{ii} = [W]_{ii}^\vee = \alpha_{ii} \in \mathbb{R}$.*

Proposition 5 enables us to rewrite problem (17) as:

$$\begin{aligned} f^* &= \min_{\tilde{\rho}, \tilde{r}} \begin{bmatrix} \tilde{\rho} \\ \tilde{r} \end{bmatrix}^\top \tilde{W} \begin{bmatrix} \tilde{\rho} \\ \tilde{r} \end{bmatrix} \\ \text{s.t.} & \quad |\tilde{r}_i|^2 = 1, \quad i = 1, \dots, n. \end{aligned} \quad (23)$$

We call \tilde{W} the *complex (anchored) pose graph matrix*. Clearly, the matrix \tilde{W} preserves the same block structure of W in (16):

$$\tilde{W} \doteq \begin{bmatrix} L & \tilde{S} \\ \tilde{S}^* & \tilde{Q} \end{bmatrix} \quad (24)$$

where \tilde{S}^* is the conjugate transpose of \tilde{S} , and $L \doteq A^\top A$ where A is the anchored incidence matrix. In Section 4 we apply Lagrangian duality to the problem (23). Before that, we provide results to characterize the spectrum of the matrices W and \tilde{W} , drawing connections with the recent literature on unit gain graphs, [60].

3.4 Analysis of the real and complex pose graph matrices

In this section we take a closer look at the structure and the properties of the real and the complex pose graph matrices W and \tilde{W} . In analogy with (13) and (16), we write \tilde{W} as

$$\tilde{W} = \begin{bmatrix} A^\top A & A^\top \tilde{D} \\ (A^\top \tilde{D})^* & \tilde{U}^* \tilde{U} + \tilde{D}^* \tilde{D} \end{bmatrix} = \begin{bmatrix} A & \tilde{D} \\ 0 & \tilde{U} \end{bmatrix}^* \begin{bmatrix} A & \tilde{D} \\ 0 & \tilde{U} \end{bmatrix} \quad (25)$$

where $\tilde{U} \in \mathbb{C}^{m \times n}$ and $\tilde{D} \in \mathbb{C}^{m \times n}$ are the “complex versions” of \bar{U} and \bar{D} in (13), i.e., they are obtained as $\tilde{U}_{ij} = [\bar{U}]_{ij}^\vee$ and $\tilde{D}_{ij} = [\bar{D}]_{ij}^\vee$, $\forall i, j$.

The factorization (25) is interesting, as it allows to identify two important matrices that compose \tilde{W} : the first is A , the anchored incidence matrix that we introduced earlier; the second is \tilde{U} which is a generalization of the incidence matrix, as specified by Definition 2 and Lemma 1 in the following. Fig. 3 reports the matrices A and \tilde{U} for a toy example with four poses.

Definition 2 (Unit gain graphs) A unit gain graph (see, e.g., [60]) is a graph in which to each orientation of an edge (i, j) is assigned a complex number \tilde{z}_{ij} (with $|\tilde{z}_{ij}| = 1$), which is the inverse of the complex number $\frac{1}{\tilde{z}_{ij}}$ assigned to the opposite orientation (j, i) . Moreover, a complex incidence matrix of a unit gain graph is a matrix in which each row corresponds to an edge and the row corresponding to edge $e = (i, j)$ has $-\tilde{z}_{ij}$ on the i -th column, $+1$ on the j -th column, and zero elsewhere.

Roughly speaking, a unit gain graph describes a problem in which we can “flip” the orientation of an edge by inverting the corresponding complex weight. To understand what this property means in our context, recall the

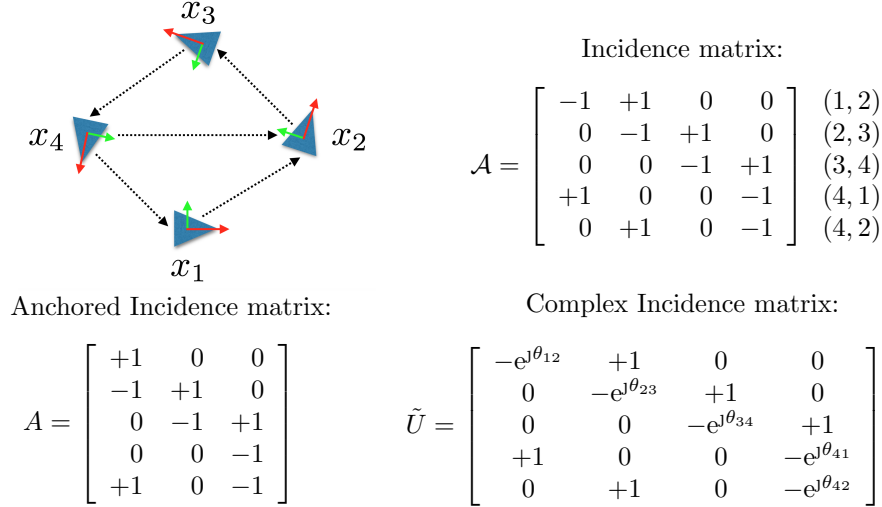


Figure 3: Example of incidence matrix, anchored incidence matrix, and complex incidence matrix, for the toy PGO problem on the top left. If $R_{ij} = R(\theta_{ij})$ is the relative rotation measurement associated to edge (i, j) , then the matrix \tilde{U} can be seen as the incidence matrix of a unit gain graph with gain $e^{j\theta_{ij}}$ associated to each edge (i, j) .

definition (12), and consider the following chain of equalities:

$$\|\bar{U}r\|_2^2 = \sum_{(i,j) \in \mathcal{E}} \|r_j - R_{ij}r_i\|_2^2 = \sum_{(i,j) \in \mathcal{E}} \|r_i - R_{ij}^\top r_j\|_2^2 \quad (26)$$

which, written in the complex domain become:

$$\|\tilde{U}\tilde{r}\|_2^2 = \sum_{(i,j) \in \mathcal{E}} |\tilde{r}_j - e^{j\theta_{ij}}\tilde{r}_i|^2 = \sum_{(i,j) \in \mathcal{E}} |\tilde{r}_i - e^{-j\theta_{ij}}\tilde{r}_j|^2 = \sum_{(i,j) \in \mathcal{E}} |\tilde{r}_i - \frac{1}{e^{j\theta_{ij}}}\tilde{r}_j|^2 \quad (27)$$

Eq. (27) essentially says that the term $\|\tilde{U}\tilde{r}\|_2^2$ does not change if we flip the orientation of an edge and invert the relative rotation measurement. The proof of the following lemma is straightforward from (27).

Lemma 1 (Properties of \tilde{U}) *Matrix \tilde{U} is a complex incidence matrix of a unit gain graph with weights $R_{ij}^\vee = e^{j\theta_{ji}}$ associated to each edge (i, j) .*

Our interest towards unit gain graphs is motivated by the recent results in [60] on the spectrum of the incidence matrix of those graphs. Using these results, we can characterize the presence of eigenvalues in zero for the matrix \tilde{W} , as specified in the following proposition (proof in Appendix 8.5).

Proposition 6 (Zero eigenvalues in \tilde{W}) *The complex anchored pose graph matrix \tilde{W} has a single eigenvalue in zero if and only if the pose graph is balanced or is a tree.*

Besides analyzing the spectrum of \tilde{W} , it is of interest to understand how the complex matrix \tilde{W} relates to the real matrix W . The following proposition states that there is a tight correspondence between the eigenvalues of the real pose graph matrix W and its complex counterpart \tilde{W} .

Proposition 7 (Spectrum of complex graph matrices) *The $2(2n-1)$ eigenvalues of W are the $2n-1$ eigenvalues of \tilde{W} , repeated twice.*

See Appendix 8.6 for a proof.

4 Lagrangian duality in PGO

In the previous section we wrote the PGO problem in complex variables as per eq. (23). In the following, we refer to this problem as the *primal* PGO problem, that, defining $\tilde{x} \doteq [\tilde{\rho}^\top \tilde{r}^\top]^\top$, can be written in compact form as

$$\begin{aligned} f^* = \min_{\tilde{x}} \quad & \tilde{x}^\top \tilde{W} \tilde{x} && \text{(Primal problem)} \\ \text{s.t.:} \quad & |\tilde{x}_i|^2 = 1, \quad i = n, \dots, 2n-1, \end{aligned} \quad (28)$$

In this section we derive the Lagrangian dual of (28), which is given in Section 4.1. Then, in Section 4.2, we discuss an SDP relaxation of (28), that can be interpreted as the dual of the dual problem. Finally, in Section 4.3 we analyze the properties of the dual problem, and discuss how it relates with the primal PGO problem.

4.1 The dual problem

The Lagrangian of the primal problem (28) is

$$\mathbb{L}(\tilde{x}, \lambda) = \tilde{x}^\top \tilde{W} \tilde{x} + \sum_{i=1}^n \lambda_i (1 - |\tilde{x}_{n+i-1}|^2)$$

where $\lambda_i \in \mathbb{R}$, $i = 1, \dots, n$, are the *Lagrange multipliers* (or *dual variables*). Recalling the structure of \tilde{W} from (24), the Lagrangian becomes:

$$\mathbb{L}(\tilde{x}, \lambda) = \tilde{x}^\top \begin{bmatrix} L & \tilde{S} \\ \tilde{S}^* & \tilde{Q}(\lambda) \end{bmatrix} \tilde{x} + \sum_{i=1}^n \lambda_i = \tilde{x}^\top \tilde{W}(\lambda) \tilde{x} + \sum_{i=1}^n \lambda_i,$$

where for notational convenience we defined

$$\tilde{Q}(\lambda) \doteq \tilde{Q} - \text{diag}(\lambda_1, \dots, \lambda_n), \quad \tilde{W}(\lambda) \doteq \begin{bmatrix} L & \tilde{S} \\ \tilde{S}^* & \tilde{Q}(\lambda) \end{bmatrix}$$

The *dual function* $d : \mathbb{R}^n \rightarrow \mathbb{R}$ is the infimum of the Lagrangian with respect to \tilde{x} :

$$d(\lambda) = \inf_{\tilde{x}} \mathbb{L}(\tilde{x}, \lambda) = \inf_{\tilde{x}} \tilde{x}^\top \tilde{W}(\lambda) \tilde{x} + \sum_{i=1}^n \lambda_i, \quad (29)$$

For any choice of λ the dual function provides a lower bound on the optimal value of the primal problem [7, Section 5.1.3]. Therefore, the *Lagrangian dual problem* looks for a *maximum* of the dual function over λ :

$$d^* \doteq \max_{\lambda} d(\lambda) = \max_{\lambda} \inf_{\tilde{x}} \tilde{x}^\top \tilde{W}(\lambda) \tilde{x} + \sum_{i=1}^n \lambda_i, \quad (30)$$

The infimum over \tilde{x} of $\mathbb{L}(\tilde{x}, \lambda)$ drifts to $-\infty$ unless $\tilde{W}(\lambda) \succeq 0$. Therefore we can safely restrict the maximization to vectors λ that are such that $\tilde{W}(\lambda) \succeq 0$; these are called *dual-feasible*. Moreover, at any dual-feasible λ , the \tilde{x} minimizing the Lagrangian are those that make $\tilde{x}^\top \tilde{W}(\lambda) \tilde{x} = 0$. Therefore, (30) reduces to the following *dual problem*

$$d^* = \max_{\lambda} \sum_i \lambda_i, \quad (\text{Dual problem}) \\ \text{s.t.: } \tilde{W}(\lambda) \succeq 0. \quad (31)$$

The importance of the dual problem is twofold. First, it holds that

$$d^* \leq f^* \quad (32)$$

This property is called *weak duality*, see, e.g., [7, Section 5.2.2]. For particular problems the inequality (32) becomes an equality, and in such cases we say that *strong duality* holds. Second, since $d(\lambda)$ is concave (minimum of affine functions), the dual problem (31) is always convex in λ , regardless the convexity properties of the primal problem. The dual PGO problem (31) is a semidefinite program (SDP).

For a given λ , we denote by $\mathcal{X}(\lambda)$ the set of \tilde{x} that attain the optimal value in problem (29), if any:

$$\mathcal{X}(\lambda) \doteq \{\tilde{x}_\lambda \in \mathbb{C}^{2n-1} : \mathbb{L}(\tilde{x}_\lambda, \lambda) = \min_{\tilde{x}} \mathbb{L}(\tilde{x}, \lambda) = \min_{\tilde{x}} \tilde{x}^\top \tilde{W}(\lambda) \tilde{x}\}$$

Since we already observed that for any dual-feasible λ the points \tilde{x} that minimize the Lagrangian are such that $\tilde{x}^\top \tilde{W}(\lambda) \tilde{x} = 0$, it follows that:

$$\mathcal{X}(\lambda) = \{\tilde{x} \in \mathbb{C}^{2n-1} : \tilde{W}(\lambda) \tilde{x} = 0\} = \text{Kernel}(\tilde{W}(\lambda)), \quad \text{for } \lambda \text{ dual-feasible.} \quad (33)$$

The following result ensures that if a vector in $\mathcal{X}(\lambda)$ is feasible for the primal problem, then it is also an optimal solution for the PGO problem.

Theorem 1 *Given $\lambda \in \mathbb{R}^n$, if an $\tilde{x}_\lambda \in \mathcal{X}(\lambda)$ is primal feasible, then \tilde{x}_λ is primal optimal; moreover, λ is dual optimal, and the duality gap is zero.*

A proof of this theorem is given in Appendix 8.7.

4.2 SDP relaxation and the dual of the dual

We have seen that a lower bound d^* on the optimal value f^* of the primal (28) can be obtained by solving the Lagrangian dual problem (31). Here, we outline another, direct, relaxation method to obtain such bound.

Observing that $\tilde{x}^\top \tilde{W} \tilde{x} = \text{Tr}(\tilde{W} \tilde{x} \tilde{x}^\top)$, we rewrite (28) equivalently as

$$\begin{aligned} f^* &= \min_{\tilde{X}, \tilde{x}} \text{Tr } \tilde{W} \tilde{X} & (34) \\ \text{s.t.: } & \text{Tr } E_i \tilde{X} = 1, \quad i = n, \dots, 2n-1, \\ & \tilde{X} = \tilde{x} \tilde{x}^\top. \end{aligned}$$

where E_i is a matrix that is zero everywhere, except for the i -th diagonal element, which is one. The condition $\tilde{X} = \tilde{x} \tilde{x}^\top$ is equivalent to (i) $\tilde{X} \succeq 0$ and (ii) \tilde{X} has rank one. Thus, (34) is rewritten by eliminating \tilde{x} as

$$\begin{aligned} f^* &= \min_{\tilde{X}} \text{Tr } \tilde{W} \tilde{X} & (35) \\ \text{s.t.: } & \text{Tr } E_i \tilde{X} = 1, \quad i = n, \dots, 2n-1, \\ & \tilde{X} \succeq 0 \\ & \text{rank}(\tilde{X}) = 1. \end{aligned}$$

Dropping the rank constraint, which is non-convex, we obtain the following SDP relaxation (see, e.g., [80]) of the primal problem:

$$\begin{aligned} s^* &= \min_{\tilde{X}} \text{Tr } \tilde{W} \tilde{X} & (36) \\ \text{s.t.: } & \text{Tr } E_i \tilde{X} = 1, \quad i = n, \dots, 2n-1, \\ & \tilde{X} \succeq 0 \end{aligned}$$

which we can also rewrite as

$$\begin{aligned}
s^* = \min_{\tilde{X}} \quad & \text{Tr } \tilde{W} \tilde{X} && \text{(SDP relaxation)} \\
\text{s.t.} \quad & \tilde{X}_{ii} = 1, \quad i = n, \dots, 2n-1, \\
& \tilde{X} \succeq 0
\end{aligned} \tag{37}$$

where \tilde{X}_{ii} denotes the i -th diagonal entry in \tilde{X} . Obviously, $s^* \leq f^*$, since the feasible set of (37) contains that of (35). One may then ask what is the relation between the Lagrangian dual and the SDP relaxation of problem (37): the answer is that the former is the dual of the latter hence, under constraint qualification, it holds that $s^* = d^*$, i.e., the SDP relaxation and the Lagrangian dual approach yield the *same* lower bound on f^* . This is formalized in the following proposition.

Proposition 8 *The Lagrangian dual of problem (37) is problem (31), and vice-versa. Strong duality holds between these two problems, i.e., $d^* = s^*$. Moreover, if the optimal solution \tilde{X}^* of (37) has rank one, then $s^* = f^*$, and hence $d^* = f^*$.*

Proof. The fact that the SDPs (37) and (31) are related by duality can be found in standard textbooks (e.g. [7, Example 5.13]); moreover, since these are convex programs, under constraint qualification, the duality gap is zero, i.e., $d^* = s^*$. To prove that $\text{rank}(\tilde{X}^*) = 1 \Rightarrow s^* = d^* = f^*$, we observe that (i) $\text{Tr } \tilde{W} \tilde{X}^* \doteq s^* \leq f^*$ since (37) is a relaxation of (35). However, when $\text{rank}(\tilde{X}^*) = 1$, \tilde{X}^* is feasible for problem (37), hence, by optimality of f^* , it holds (ii) $f^* \leq f(\tilde{X}^*) = \text{Tr } \tilde{W} \tilde{X}^*$. Combining (i) and (ii) we prove that, when $\text{rank}(\tilde{X}^*) = 1$, then $f^* = s^*$, which also implies $f^* = d^*$. \square

To the best of our knowledge this is the first time in which the SDP relaxation has been proposed to solve PGO. For the rotation subproblem, SDP relaxations have been proposed in [71, 66, 33]. According to Proposition 8, one advantage of the SDP relaxation approach is that we can a-posteriori check if the duality (or, in this case, the relaxation) gap is zero, from the optimal solution \tilde{X}^* . Indeed, if one solves (37) and finds that the optimal \tilde{X}^* has rank one, then we actually solved (28), hence the relaxation gap is zero. Moreover, in this case, from spectral decomposition of \tilde{X}^* we can get a vector \tilde{x}^* such that $\tilde{X}^* = (\tilde{x}^*)(\tilde{x}^*)^*$, and this vector is an optimal solution to the primal problem.

In the following section we derive similar a-posteriori conditions for the dual problem (31). These conditions enable the computation of a primal optimal solution. Moreover, they allow discussing the uniqueness of such

solution. Furthermore, we prove that in special cases we can provide *a-priori* conditions that guarantee that the duality gap is zero.

4.3 Analysis of the dual problem

In this section we provide conditions under which the duality gap is zero. These conditions depend on the spectrum of $\tilde{W}(\lambda^*)$, which arises from the solution of (31). We refer to $\tilde{W}(\lambda^*)$ as the *penalized pose graph matrix*. A first proposition establishes that (31) attains an optimal solution.

Proposition 9 *The optimal value d^* in (31) is attained at a finite λ^* . Moreover, the penalized pose graph matrix $\tilde{W}(\lambda^*)$ has an eigenvalue in 0.*

Proof. Since $\tilde{W}(\lambda) \succeq 0$ implies that the diagonal entries are nonnegative, the feasible set of (31) is contained in the set $\{\lambda : \tilde{W}_{ii} - \lambda_i \geq 0, i = 1, \dots, 2n - 1\}$ (recall that \tilde{W}_{ii} are reals according to Remark 2). On the other hand, $\lambda_l = 0_{2n-1}$ is feasible and all points in the set $\{\lambda : \lambda_i \geq 0$ yield an objective that is at least as good as the objective value at λ_l . Therefore, the problem is equivalent to $\max_{\lambda} \sum_i \lambda_i$ subject to the original constraint, plus a box constraint on $\lambda \in \{0 \leq \lambda_i \leq \tilde{W}_{ii}, i = 1, \dots, n\}$. Thus we maximize a linear function over a compact set, hence a finite optimal solution λ^* must be attained.

Now let us prove that $\tilde{W}(\lambda^*)$ has an eigenvalue in zero. Assume by contradiction that $\tilde{W}(\lambda^*) \succ 0$. From the Schur complement rule we know:

$$\tilde{W}(\lambda^*) \succ 0 \Leftrightarrow \begin{cases} L \succ 0 \\ \tilde{Q}(\lambda^*) - \tilde{S}^* L^{-1} \tilde{S} \succ 0 \end{cases} \quad (38)$$

The condition $L \succ 0$ is always satisfied for a connected graph, since $L = A^\top A$, and the anchored incidence matrix A , obtained by removing a node from the original incidence matrix, is always full-rank for connected graphs [67, Section 19.3]. Therefore, our assumption $\tilde{W}(\lambda^*) \succ 0$ implies that

$$\tilde{Q}(\lambda^*) - \tilde{S}^* L^{-1} \tilde{S} = \tilde{Q} - \tilde{S}^* L^{-1} \tilde{S} - \text{diag}(\lambda^*) \succ 0 \quad (39)$$

Now, let

$$\epsilon = \lambda_{\min}(\tilde{Q}(\lambda^*) - \tilde{S}^* L^{-1} \tilde{S}) > 0.$$

which is positive by the assumption $\tilde{W}(\lambda^*) \succ 0$. Consider $\lambda = \lambda^* + \epsilon \mathbf{1}$, then

$$\tilde{Q}(\lambda) - \tilde{S}^* L^{-1} \tilde{S} = \tilde{Q}(\lambda) - \tilde{S}^* L^{-1} \tilde{S} - \epsilon I \succeq 0,$$

thus λ is dual feasible, and $\sum_i \lambda_i > \sum_i \lambda_i^*$, which would contradict optimality of λ^* . We thus proved that $\tilde{Q}(\lambda^*)$ must have a zero eigenvalue. \square

Proposition 10 (No duality gap) *If the zero eigenvalue of the penalized pose graph matrix $\tilde{W}(\lambda^*)$ is simple then the duality gap is zero, i.e., $d^* = f^*$.*

Proof. We have already observed in Proposition 8 that (37) is the dual problem of (31), therefore, we can interpret \tilde{X} as a Lagrange multiplier for the constraint $\tilde{W}(\lambda) \succeq 0$. If we consider the optimal solutions \tilde{X}^* and λ^* of (37) and (31), respectively, the *complementary slackness* condition ensures that $\text{Tr}(\tilde{W}(\lambda^*)\tilde{X}^*) = 0$ (see [7, Example 5.13]). Let us parametrize $\tilde{X}^* \succeq 0$ as

$$\tilde{X}^* = \sum_{i=1}^{2n-1} \mu_i \tilde{v}_i \tilde{v}_i^*,$$

where $0 \leq \mu_1 \leq \mu_2 \leq \dots \leq \mu_{2n-1}$ are the eigenvalues of \tilde{X} , and \tilde{v}_i form a unitary set of eigenvectors. Then, the complementary slackness condition becomes

$$\begin{aligned} \text{Tr}(\tilde{W}(\lambda^*)\tilde{X}^*) &= \text{Tr}\left(\tilde{W}(\lambda^*) \sum_{i=1}^{2n-1} \mu_i \tilde{v}_i \tilde{v}_i^*\right) \\ &= \sum_{i=1}^{2n-1} \mu_i \text{Tr}\left(\tilde{W}(\lambda^*) \tilde{v}_i \tilde{v}_i^*\right) \\ &= \sum_{i=1}^{2n-1} \mu_i \tilde{v}_i^* \tilde{W}(\lambda^*) \tilde{v}_i = 0. \end{aligned}$$

Since $\tilde{W}(\lambda^*) \succeq 0$, the above quantity is zero at a nonzero \tilde{X}^* (\tilde{X}^* cannot be zero since it needs to satisfy the constraints $\tilde{X}_{ii} = 1$) if and only if $\mu_i = 0$ for $i = m+1, \dots, 2n-1$, and $\tilde{W}(\lambda^*) \tilde{v}_i = 0$ for $i = 1, \dots, m$, where m is the multiplicity of 0 as an eigenvalue of $\tilde{W}(\lambda^*)$. Hence \tilde{X}^* has the form

$$\tilde{X}^* = \sum_{i=1}^m \mu_i \tilde{v}_i \tilde{v}_i^*, \quad (40)$$

where \tilde{v}_i , $i = 1, \dots, m$, form a unitary basis of the null-space of $\tilde{W}(\lambda^*)$. Now, if $m = 1$, then the solution \tilde{X}^* to problem (37) has rank one, but according to Proposition 8 this implies $d^* = f^*$, proving the claim. \square

In the following we say that $\tilde{W}(\lambda^*)$ satisfies the *single zero eigenvalue property* (SZEP) if its zero eigenvalue is simple. The following corollary provides a more explicit relation between the solution of the primal and the dual problem when $\tilde{W}(\lambda^*)$ satisfies the SZEP.

Corollary 1 (SZEP $\Rightarrow \tilde{x}^* \in \mathcal{X}(\lambda^*)$) *If the zero eigenvalue of $\tilde{W}(\lambda^*)$ is simple, then the set $\mathcal{X}(\lambda^*)$ contains a primal optimal solution. Moreover, the primal optimal solution is unique, up to an arbitrary rotation.*

Proof. Let \tilde{x}^* be a primal optimal solution, and let $f^* = (\tilde{x}^*)^* \tilde{W}(\tilde{x}^*)$ be the corresponding optimal value. From Proposition 10 we know that the SZEP implies that the duality gap is zero, i.e., $d^* = f^*$, hence

$$\sum_{i=1}^n \lambda_i^* = (\tilde{x}^*)^* \tilde{W}(\tilde{x}^*). \quad (41)$$

Since \tilde{x}^* is a solution of the primal, it must be feasible, hence $|\tilde{x}_i^*|^2 = 1$, $i = n, \dots, 2n - 1$. Therefore, the following equalities holds:

$$\sum_{i=1}^n \lambda_i^* = \sum_{i=1}^n \lambda_i^* |\tilde{x}_{n+i-1}^*|^2 = (\tilde{x}^*)^* \begin{bmatrix} 0 & 0 \\ 0 & \text{diag}(\lambda^*) \end{bmatrix} (\tilde{x}^*) \quad (42)$$

Plugging (42) back into (41):

$$(\tilde{x}^*)^* \left[\tilde{W} - \begin{bmatrix} 0 & 0 \\ 0 & \text{diag}(\lambda^*) \end{bmatrix} \right] (\tilde{x}^*) = 0 \Leftrightarrow (\tilde{x}^*)^* \tilde{W}(\lambda^*) (\tilde{x}^*) = 0 \quad (43)$$

which proves that \tilde{x}^* belongs to the null space of $\tilde{W}(\lambda^*)$, which coincides with our definition of $\mathcal{X}(\lambda^*)$ in (33), proving the first claim.

Let us prove the second claim. From the first claim we know that the SZEP implies that any primal optimal solution is in $\mathcal{X}(\lambda^*)$. Moreover, when $\tilde{W}(\lambda^*)$ has a single eigenvalue in zero, then $\mathcal{X}(\lambda^*) = \text{Kernel}(\tilde{W}(\lambda^*))$ is 1-dimensional and can be written as $\mathcal{X}(\lambda^*) = \{\tilde{\gamma} \tilde{x}^* : \tilde{\gamma} \in \mathbb{C}\}$, or, using the polar form for $\tilde{\gamma}$:

$$\mathcal{X}(\lambda^*) = \{\eta e^{j\varphi} \tilde{x}^* : \eta, \varphi \in \mathbb{R}\} \quad (44)$$

From (44) it's easy to see that any $\eta \neq 1$ would alter the norm of \tilde{x}^* , leading to a solution that it's not primal feasible. On the other hand, any $e^{j\varphi} \tilde{x}^*$ belongs to $\mathcal{X}(\lambda^*)$, and it's primal feasible ($|e^{j\varphi} \tilde{x}_i^*| = |\tilde{x}_i^*|$), hence by Theorem 1, any $e^{j\varphi} \tilde{x}^*$ is primal optimal. We conclude the proof by noting that the multiplication by $e^{j\varphi}$ corresponds to a global rotation of the pose estimate \tilde{x}^* : this can be easily understood from the relation (18). \square

Proposition 10 provides an *a-posteriori* condition on the duality gap, that requires solving the dual problem; while Section 6 will show that this condition is very useful in practice, it is also interesting to devise a-priori conditions, that can be assessed from the pose graph matrix \tilde{W} , without solving the dual problem. A first step in this direction is the following proposition.

Proposition 11 (Strong duality in trees and balanced pose graphs)

Strong duality holds for any balanced pose graph optimization problem, and for any pose graph whose underlying graph is a tree.

Proof. Balanced pose graphs and trees have in common the fact that they attain $f^* = 0$ (Propositions 1-2). By weak duality we know that $d^* \leq 0$. However, $\lambda = 0_n$ is feasible (as $\tilde{W} \succeq 0$) and attains $d(\lambda) = 0$, hence $\lambda = 0_n$ is feasible and dual optimal, proving $d^* = f^*$. \square

5 Algorithms

In this section we exploit the results presented so far to devise an algorithm to solve PGO. The idea is to solve the dual problem, and use λ^* and $\tilde{W}(\lambda^*)$ to compute a solution for the primal PGO problem. We split the presentation into two sections: Section 5.1 discusses the case in which $\tilde{W}(\lambda^*)$ satisfies the SZEP, while Section 5.2 discusses the case in which $\tilde{W}(\lambda^*)$ has multiple eigenvalues in zero. This distinction is important as in the former case (which is the most common in practice) we can compute a provably optimal solution for PGO, while in the latter case our algorithm returns an estimate that is not necessarily optimal. Finally, in Section 5.3 we summarize our algorithm and present the corresponding pseudocode.

5.1 Case 1: $\tilde{W}(\lambda^*)$ satisfies the SZEP

According to Corollary 1, if $\tilde{W}(\lambda^*)$ has a single zero eigenvalue, then the optimal solution of the primal problem \tilde{x}^* is in $\mathcal{X}(\lambda^*)$, where $\mathcal{X}(\lambda^*)$ coincides with the null space of $\tilde{W}(\lambda^*)$, as per (33). Moreover, this null space is 1-dimensional, hence it can be written explicitly as:

$$\mathcal{X}(\lambda^*) = \text{Kernel}(\tilde{W}(\lambda^*)) = \{\tilde{v} \in \mathbb{C}^{2n-1} : \tilde{v} = \gamma \tilde{x}^*\}, \quad (45)$$

which means that any vector in the null space is a scalar multiple of the primal optimal solution \tilde{x}^* . This observation suggests a computational approach to compute \tilde{x}^* . We can first compute an eigenvector \tilde{v} corresponding to the single zero eigenvalue of $\tilde{W}(\lambda^*)$ (this is a vector in the null space of $\tilde{W}(\lambda^*)$). Then, since \tilde{x}^* must be primal feasible (i.e., $|\tilde{x}_n| = \dots = |\tilde{x}_{2n-1}| = 1$), we compute a suitable scalar γ that makes $\frac{1}{\gamma} \tilde{v}$ primal feasible. This scalar is clearly $\gamma = |\tilde{v}_n| = \dots = |\tilde{v}_{2n-1}|$ (we essentially need to normalize the norm of the last n entries of \tilde{v}). The existence of a suitable γ , and hence the fact that $|\tilde{v}_n| = \dots = |\tilde{v}_{2n-1}| > 0$, is guaranteed by Corollary 1. As a result we

get the optimal solution $\tilde{x}^* = \frac{1}{\gamma}\tilde{v}$. The pseudocode of our approach is given in Algorithm 1, and further discussed in Section 5.3.

5.2 Case 2: $\tilde{W}(\lambda^*)$ does *not* satisfy the SZEP

Currently we are not able to compute a guaranteed optimal solution for PGO, when $\tilde{W}(\lambda^*)$ has multiple eigenvalues in zero. Nevertheless, it is interesting to exploit the solution of the dual problem for finding a (possibly suboptimal) estimate, which can be used, for instance, as initial guess for an iterative technique.

Eigenvector method. One idea to compute a suboptimal solution from the dual problem is to follow the same approach of Section 5.1: we compute an eigenvector of $\tilde{W}(\lambda^*)$, corresponding to one of the zero eigenvalues, and we normalize it to make it feasible. In this case, we are not guaranteed that $|\tilde{v}_n| = \dots = |\tilde{v}_{2n-1}| > 0$ (as in the previous section), hence the normalization has to be done component-wise, for each of the last n entries of \tilde{v} . In the following, we consider an alternative approach, which we have seen to perform better in practice (see experiments in Section 6).

Null space method. This approach is based on the insight of Theorem 1: if there is a primal feasible $\tilde{x} \in \mathcal{X}(\lambda^*)$, then \tilde{x} must be primal optimal. Therefore we look for a vector $\tilde{x} \in \mathcal{X}(\lambda^*)$ that is “close” to the feasible set. According to (33), $\mathcal{X}(\lambda^*)$ coincides with the null space of $\tilde{W}(\lambda^*)$. Let us denote with $\tilde{V} \in \mathbb{C}^{(2n-1) \times q}$ a basis of the null space of $\tilde{W}(\lambda^*)$, where q is the number of zero eigenvalues of $\tilde{W}(\lambda^*)$.⁴ Any vector \tilde{x} in the null space of $\tilde{W}(\lambda^*)$ can be written as $\tilde{x} = \tilde{V}\tilde{z}$, for some vector $\tilde{z} \in \mathbb{C}^q$. Therefore we propose to compute a possibly suboptimal estimate $\tilde{x} = \tilde{V}\tilde{z}^*$, where \tilde{z}^* solves the following optimization problem:

$$\begin{aligned} \max_{\tilde{z}} \quad & \sum_{i=1}^{2n-1} \text{real}(\tilde{V}_i\tilde{z}) + \text{imag}(\tilde{V}_i\tilde{z}) \\ \text{s.t.} \quad & |\tilde{V}_i\tilde{z}|^2 \leq 1, \quad i = n, \dots, 2n-1 \end{aligned} \quad (46)$$

where \tilde{V}_i denotes the i -th row of \tilde{V} , and $\text{real}(\cdot)$ and $\text{imag}(\cdot)$ return the real and the imaginary part of a complex number, respectively. For an intuitive explanation of problem (46), we notice that the feasible set of the primal problem (28) is described by $|\tilde{x}_i|^2 = 1$, for $i = n, \dots, 2n-1$. In problem (46) we relax the equality constraints to convex inequality constraints $|\tilde{x}_i|^2 \leq 1$, for $i = n, \dots, 2n-1$; these can be written as $|\tilde{V}_i\tilde{z}|^2 \leq 1$, recalling that we

⁴ \tilde{V} can be computed from singular value decomposition of $\tilde{W}(\lambda^*)$.

are searching in the null space of $\tilde{W}(\lambda^*)$, which is spanned by $\tilde{V}\tilde{z}$. Then, the objective function in (46) encourages “large” elements $\tilde{V}_i\tilde{z}$, hence pushing the inequality $|\tilde{V}_i\tilde{z}|^2 \leq 1$ to be tight. While other metrics can force large entries $\tilde{V}_i\tilde{z}$, we preferred the linear metric (46) to preserve convexity.

Note that $\tilde{x} = \tilde{V}\tilde{z}^*$, in general, is neither optimal nor feasible for our PGO problem (28), hence we need to normalize it to get a feasible estimate. The experimental section provides empirical evidence that, despite being heuristic in nature, this method performs well in practice, outperforming – among the others – the eigenvector method presented earlier in this section.

5.3 Pseudocode and implementation details

The pseudocode of our algorithm is given in Algorithm 1. The first step is to solve the dual problem, and check the a-posteriori condition of Proposition 10. If the SZEP is satisfied, then we can compute the optimal solution by scaling the eigenvector of $\tilde{W}(\lambda^*)$ corresponding to the zero eigenvalue μ_1 . This is the case described in Section 5.1 and is the most relevant in practice, since the vast majority of robotics problems falls in this case.

The “else” condition corresponds to the case in which $\tilde{W}(\lambda^*)$ has multiple eigenvalue in zero. The pseudocode implements the null space approach of Section 5.2. The algorithm computes a basis for the null space of $\tilde{W}(\lambda^*)$ and solves (46) to find a vector belonging to the null space (i.e, in the form $\tilde{x} = \tilde{V}\tilde{z}$) that is close to the feasible set. Since such vector is not guaranteed to be primal feasible (and it is not in general), the algorithm normalizes the last n entries of $\tilde{x}^* = \tilde{V}\tilde{z}^*$, so to satisfy the unit norm constraints in (28). Besides returning the estimate \tilde{x}^* , the algorithm also provides an optimality certificate when $\tilde{W}(\lambda^*)$ has a single eigenvalue in zero.

```

input : Complex PGO matrix  $\tilde{W}$ 
output: Primal solution  $\tilde{x}^*$  and optimality certificate isOpt
solve the dual problem (31) and get  $\lambda^*$  ;
if  $\tilde{W}(\lambda^*)$  has a single eigenvalue  $\mu_1$  at zero then
    compute the eigenvector  $\tilde{v}$  of  $\tilde{W}(\lambda^*)$  corresponding to  $\mu_1$ ;
    compute  $\tilde{x}^* = \frac{1}{\gamma}\tilde{v}$ , where  $\gamma = |\tilde{v}_j|$ , for any  $j \in \{n, \dots, 2n - 1\}$  ;
    set isOpt = true;
else
    compute a basis  $\tilde{V}$  for the null space of  $\tilde{W}(\lambda^*)$  using SVD;
    compute  $\tilde{z}^*$  by solving the convex problem (46);
    set  $\tilde{x}^* = \tilde{V}\tilde{z}^*$  and normalize  $|\tilde{x}_i|$  to 1, for all  $i = n, \dots, 2n - 1$ ;
    set isOpt = unknown;
end
return  $(\tilde{x}^*, \text{isOpt})$ 

```

Algorithm 1: Solving PGO using Lagrangian duality.

6 Numerical Analysis and Discussion

The objective of this section is four-fold. First, we validate our theoretical derivation, providing experimental evidence that supports the claims. Second, we show that the duality gap is zero in a vast amount of practical problems. Third, we confirm the effectiveness of Algorithm 1 to solve PGO. Fourth, we provide toy examples in which the duality gap is greater than zero, hoping that this can stimulate further investigation towards *a-priori* conditions that ensure zero duality gap.

Simulation setup. For each run we generate a random graph with $n = 10$ nodes, unless specified otherwise. We draw the position of each pose by a uniform distribution in a $10\text{m} \times 10\text{m}$ square. Similarly, ground truth node orientations are randomly selected in $(-\pi, +\pi]$. Then we create set of edges defining a spanning *path* of the graph (these are usually called *odometric edges*); moreover, we add further edges to the edge set, by connecting random pairs of nodes with probability $P_c = 0.1$ (these are usually called *loop closures*). From the randomly selected *true* poses, and for each edge (i, j) in the edge set, we generate the relative pose measurement using the following model:

$$\begin{aligned}
 \Delta_{ij} &= R_i^\top (p_j - p_i) + \epsilon_\Delta, & \epsilon_\Delta &\sim N(0_2, \sigma_\Delta^2) \\
 R_{ij} &= R_i^\top R_j R(\epsilon_R), & \epsilon_R &\sim N(0, \sigma_R^2)
 \end{aligned} \tag{47}$$

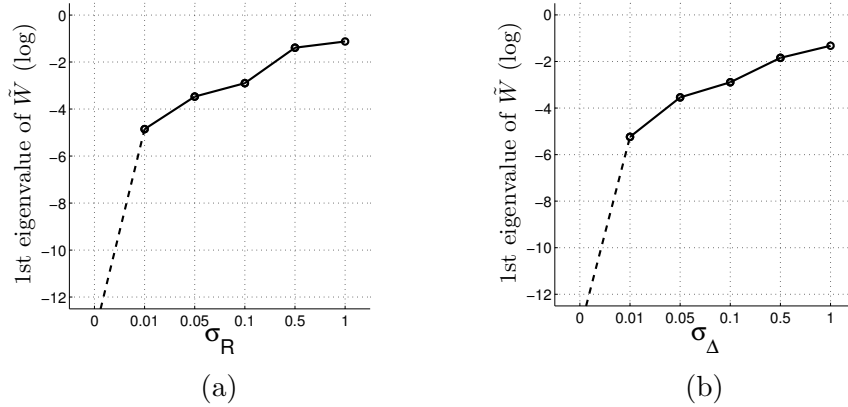


Figure 4: Smallest eigenvalue of \tilde{W} (in logarithmic scale) for different levels of (a) rotation noise (std: σ_R), and (b) translation noise (std: σ_Δ). The figure shows the minimum observed value over 100 Monte Carlo runs, for non-tree graphs. The minimum eigenvalue is zero only if the graph is balanced.

where $\epsilon_\Delta \in \mathbb{R}^2$ and $\epsilon_R \in \mathbb{R}$ are zero-mean Normally distributed random variables, with standard deviation σ_Δ and σ_R , respectively, and $R(\epsilon_R)$ is a random planar rotation of an angle ϵ_R . Unless specified otherwise, all statistics are computed over 100 runs.

Spectrum of \tilde{W} . In Proposition 6, we showed that the complex anchored pose graph matrix \tilde{W} has at most one eigenvalue in zero, and the zero eigenvalue only appears when the pose graph is balanced or is a tree.

Fig. 4(a) reports the value of the smallest eigenvalue of \tilde{W} (in log scale) for different σ_R , with fixed $\sigma_\Delta = 0$ rad. When also σ_R is zero, the pose graph is balanced, hence the smallest eigenvalue of \tilde{W} is (numerically) zero. For increasing levels of noise, the smallest eigenvalue increases and stays away from zero. Similarly, Fig. 4(b) reports the value of the smallest observed eigenvalue of \tilde{W} (in log scale) for different σ_Δ , with fixed $\sigma_R = 0$ rad.

Duality gap is zero in many cases. This section shows that for the levels of measurement noise of practical interest, the matrix $\tilde{W}(\lambda^*)$ satisfies the Single Eigenvalue Property (SZEP), hence the duality gap is zero (Proposition 10). We consider the same measurement model of Eq. (47), and we analyze the percentage of tests in which $\tilde{W}(\lambda^*)$ satisfies the SZEP.

Fig. 5(a) shows the percentage of the experiments in which the penalized

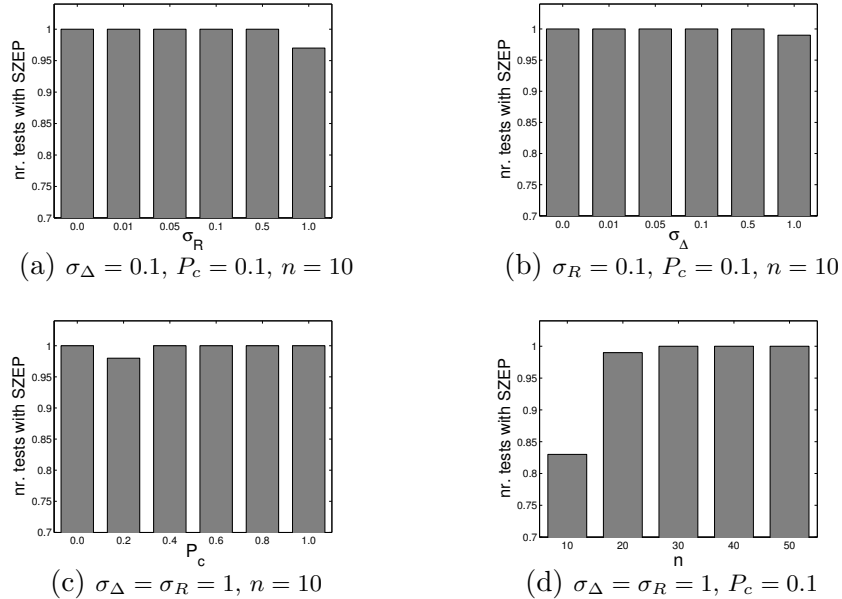


Figure 5: Percentage of problems in which $\tilde{W}(\lambda^*)$ satisfied the SZEP property, for different (a) rotation measurement noise σ_R , (b) translation measurement noises σ_{Δ} , (c) loop closure probability P_c , (d) number of nodes n .

pose graph matrix $\tilde{W}(\lambda^*)$ has a single zero eigenvalue, for different values of rotation noise σ_R , and keeping fixed the translation noise to $\sigma_{\Delta} = 0.1\text{m}$ (this is a typical value in mobile robotics applications). For $\sigma_R \leq 0.5\text{rad}$, $\tilde{W}(\lambda^*)$ satisfies the SZEP in all tests. This means that in this range of operation, Algorithm 1 is guaranteed to compute a globally-optimal solution for PGO. For $\sigma_R = 1\text{rad}$, the percentage of successful experiments drops, while still remaining larger than 90%. Note that $\sigma_R = 1\text{rad}$ is a very large rotation noise (in robotics, typically $\sigma_R \leq 0.3\text{rad}$ [13]), and it is not far from the case in which rotation measurements are uninformative (uniformly distributed in $(-\pi, +\pi]$). To push our evaluation further we also tested this extreme case. When rotation noise is uniformly distributed in $(-\pi, +\pi]$, we obtained a percentage of successful tests (single zero eigenvalue) of 69%, which confirms that the number of cases in which we can compute a globally optimal solution drops gracefully when increasing the noise levels.

Fig. 5(b) shows the percentage of the experiments in which $\tilde{W}(\lambda^*)$ has a single zero eigenvalue, for different values of translation noise σ_{Δ} , and keeping fixed the rotation noise to $\sigma_R = 0.1\text{rad}$. Also in this case, for

practical noise regimes, our approach can compute a global solution in all cases. The percentage of successful tests drops to 98% when the translation noise has standard deviation 1m. We also tested the case of uniform noise on translation measurements. When we draw the measurement noise from a uniform distribution in $[-5, 5]^2$ (recall that the poses are deployed in a 10×10 square), the percentage of successful experiments is 68%.

We also tested the percentage of experiments satisfying the SZEP for different levels of connectivity of the graph, controlled by the parameter P_c . We observed 100% successful experiments, independently on the choice of P_c , for $\sigma_R = \sigma_\Delta = 0.1$ and $\sigma_R = \sigma_\Delta = 0.5$. A more interesting case is shown in Fig. 5(c) and corresponds to the case $\sigma_R = \sigma_\Delta = 1$. The SZEP is always satisfied for $P_c = 0$: this is natural as $P_c = 0$ always produces trees, for which we are guaranteed to satisfy the SZEP (Proposition 11). For $P_c = 0.2$ the SZEP fails in few runs. Finally, increasing the connectivity beyond $P_c = 0.4$ re-establishes 100% of successful tests. This would suggest that the connectivity level of the graph influences the duality gap, and better connected graphs have more chances to have zero duality gap.

Finally, we tested the percentage of experiments satisfying the SZEP for different number of nodes n . We tested the following number of nodes: $n = \{10, 20, 30, 40, 50\}$. For $\sigma_R = \sigma_\Delta = 0.1$ and $\sigma_R = \sigma_\Delta = 0.5$ the SZEP was satisfied in 100% of the tests, and we omit the results for brevity. The more challenging case $\sigma_R = \sigma_\Delta = 1$ is shown in Fig. 5(d). The percentage of successful tests increases for larger number of poses. We remark that current SDP solvers do not scale well to large problems, hence a Monte Carlo analysis over larger problems becomes prohibitive. We refer the reader to [14] for single-run experiments on larger PGO problems, which confirm that the duality gap is zero in problems arising in real-world robotics applications.

Performance of Algorithm 1 In this section we show that Algorithm 1 provides an effective solution for PGO. When $\tilde{W}(\lambda^*)$ satisfies the SZEP, the algorithm is provably optimal, and it enables to solve problems that are already challenging for iterative solvers. When the $\tilde{W}(\lambda^*)$ does *not* satisfy the SZEP, we show that the proposed approach, while not providing performance guarantees, largely outperforms competitors.

Case 1: $\tilde{W}(\lambda^)$ satisfies the SZEP.* When $\tilde{W}(\lambda^*)$ satisfies the SZEP, Algorithm 1 is guaranteed to produce a globally optimal solution. However, one may argue that in the regime of operation in which the SZEP holds, PGO problem instances are sufficiently “easy” that commonly used iterative techniques also perform well. In this paragraph we briefly show that the SZEP

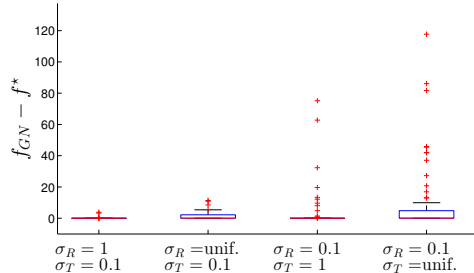


Figure 6: Statistics on tests in which the SZEP is satisfied: the figure reports the gap between the optimal objective f^* attained by Algorithm 1 and the objective f_{GN} attained by a Gauss-Newton method initialized at the true poses. We simulate different combinations of noise (see x-axis labels), keeping fixed $n = 10$ and $P_c = 0.1$. The label “unif.” denotes uniform noise for rotations (in $(-\pi, +\pi]$) or translations (in $[-5, +5]$).

is satisfied in many instances that are hard to solve. For this purpose, we focus on the most challenging cases we discussed so far, i.e., problem instances with large rotation and translation noise. Then we consider the problems in which the SZEP is satisfied and we compare the solution of Algorithm 1, which is proven to attain f^* , versus the solution of a Gauss-Newton method initialized at the *true* poses. Ground truth poses are an ideal initial guess (which is unfortunately available only in simulation): intuitively, the global minimum of the cost should be close to the ground truth poses (this is one of the motivations for maximum likelihood estimation). Fig. 6 shows the gap between the objective attained by the Gauss-Newton method (denoted as f_{GN}) and the optimal objective obtained from Algorithm 1. The figure confirms that our algorithm provides a guaranteed optimal solution in a regime that is already challenging, and in which iterative approaches may fail to converge even from a good initialization.

Case 2: $\tilde{W}(\lambda^)$ does not satisfy the SZEP.* In this case, Algorithm 1 computes an estimate, according to the *null space approach* proposed in Section 5.2; we denote this approach with the label NS. To evaluate the performance of the proposed approach, we considered 100 instances in which the SZEP was *not* satisfied and we compared our approach against the following methods: a Gauss-Newton method initialized at the ground truth poses (GN), the eigenvector method described at the beginning of Section 5.2 (Eig), and the SDP relaxation of Section 4.2 (SDP). For the SDP approach, we compute the solution \tilde{X}^* of the relaxed problem (37). If \tilde{X}^* has rank

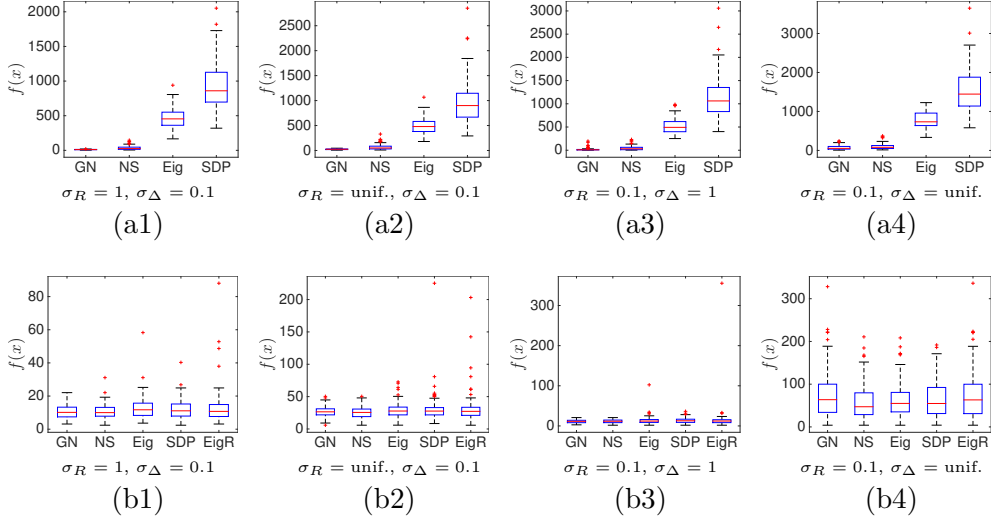


Figure 7: Statistics on tests in which the SZEP is *not* satisfied: (a1)-(a4): Comparison of different PGO solvers for different levels of noise. The compared approaches are: a Gauss-Newton method initialized at the ground truth poses (GN), the proposed null space approach (NS), the eigenvector method (Eig), the SDP relaxation (SDP). (b1)-(b4): Comparison of the techniques GN, NS, Eig, SDP, refined with a Gauss-Newton method, and an alternative approach which solves for rotations first (EigR).

larger than 1, we find the closest rank-1 matrix $\tilde{X}_{\text{rank-1}}$ from singular value decomposition [28]. Then we factorize $\tilde{X}_{\text{rank-1}}$ as $\tilde{X}_{\text{rank-1}} = \tilde{x}\tilde{x}^*$ (\tilde{x} can be computed via Cholesky factorization of $\tilde{X}_{\text{rank-1}}$ [70]). We report the results of our comparison in the first row of Fig. 7, where we show for different noise setups (sub-figures (a1) to (a4)), the cost of the estimate produced by the four approaches. The proposed null space approach (NS) largely outperforms the Eig and the SDP approaches, and has comparable performance with an “oracle” GN approach which knows the ground truth poses.

One may also compare the performance of the approaches NS, Eig, SDP after refining the corresponding estimates with a Gauss-Newton method, which tops off residual errors. The cost obtained by the different techniques, with the Gauss-Newton refinement, are shown in the second row of Fig. 7. For this case we also added one more initialization technique in the comparison: we consider an approach that solves for rotations first, using the eigenvalue method in [70], and then applies the Gauss-Newton method from

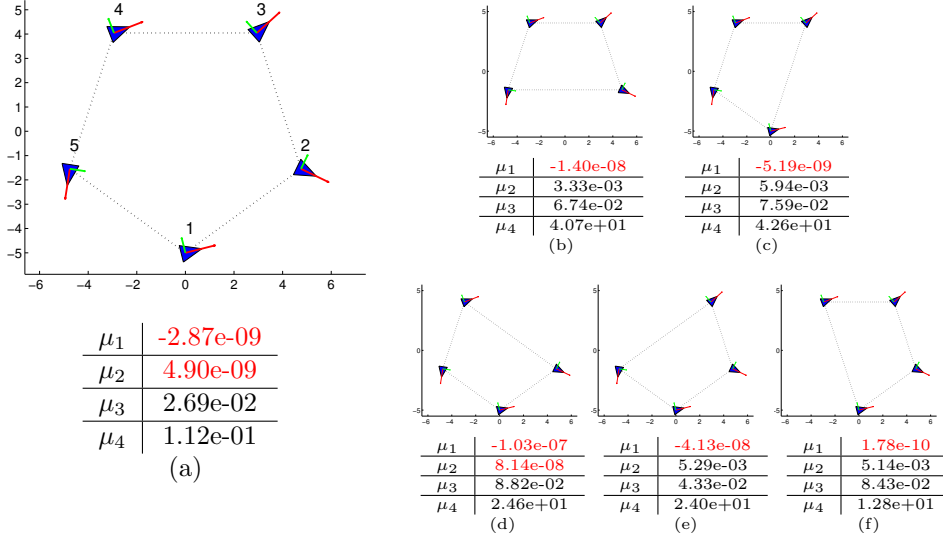


Figure 8: (a) Toy example of chain pose graph in which the SZEP fails. In each plot we also report the four smallest eigenvalues of the penalized pose graph matrix $\tilde{W}(\lambda^*)$ for the corresponding PGO problem. Removing a node from the original graph may change the duality properties of the graph. In (b), (c), (d), (e), (f) we remove nodes 1, 2, 3, 4, 5, respectively. Removing any node, except node 3, leads to a graph that satisfied the SZEP.

the rotation guess.⁵ Fig. 7(b1) to Fig. 7(b4) show less differences (in average) among the techniques, as in most cases the Gauss-Newton refinement is able to converge starting from all the compared initializations. However, for the techniques Eig, SDP, and EigR we see many red sample points, which denote cases in which the error is larger than the 75th percentile; these are the cases in which the techniques failed to converge and produced a large cost. On the other hand, the proposed NS approach is less prone to converge to a bad minimum (fewer and lower red samples).

Chain graph counterexample and discussion. In this section we consider a simple graph topology: the *chain graph*. A chain graph is a graph with edges $(1, 2), (2, 3), \dots, (n-1, n), (n, 1)$. Removing the last edge we obtain a tree (or, more specifically, a *path*), for which the SZEP is always satisfied. Therefore the question is: *is the SZEP always satisfied in PGO whose*

⁵This was not included in the first row of Fig. 7 as it does not provide a guess for the positions of the nodes.

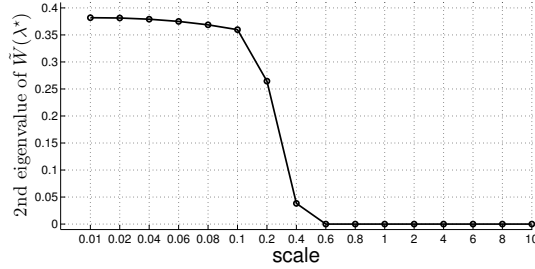


Figure 9: Second eigenvalue of the matrix $\tilde{W}(\lambda^*)$ for different variations of the toy graph of Fig. 8(a). Each variation is obtained by scaling the translation measurements of the original graph by the amount specified on the x-axis of this figure. When the scale of the measurement is ≤ 0.4 the second eigenvalue of $\tilde{W}(\lambda^*)$ is larger than zero, hence the SZEP is satisfied.

underlying graph is a chain? The answer, unfortunately, is no. Fig. 8(a) provides an example of a very simple chain graph with 5 nodes that fails to meet the SZEP property. The figure reports the 4 smallest eigenvalues of $\tilde{W}(\lambda^*)$ (μ_1, \dots, μ_4), and the first two are numerically zero.

If the chain graph were balanced, Proposition 11 says that the SZEP needs to be satisfied. Therefore, one may argue that failure to meet the SZEP depends on the amount of error accumulated along the loop in the graph. Surprisingly, also this intuition fails. In Fig. 8(b-f) we show the pose graphs obtained by removing a single node from the pose graph in Fig. 8(a). When removing a node, say k , we introduce a relative measurement between nodes $k - 1$ and $k + 1$, that is equal to the composition of the relative measurements associated to the edges $(k - 1, k)$ and $(k, k + 1)$ in the original graph. By constructions, the resulting graphs have the same accumulated errors (along each loop) as the original graph. However, interestingly, they do not necessarily share the same duality properties of the original graph. The graphs obtained by removing nodes 1, 2, 4, 5 (shown in figures b,c,e,f, respectively), in fact, satisfy the SZEP. On the other hand, the graph in Fig. 8(c) still has 2 eigenvalues in zero. The data to reproduce these toy examples are reported in Appendix 8.8.

We conclude with a test showing that the SZEP is not only dictated by the underlying rotation subproblem but also depends heavily on the translation part of the optimization problem. To show this we consider variations of the PGO problem in Fig. 8(a), in which we “scale” all translation measurements by a constant factor. When the scale factor is smaller than one we obtain a PGO problem in which nodes are closer to each other; for scale

> 1 we obtain larger inter-nodal measurements; the scale equal to 1 coincides with the original problem. Fig 9 shows the second eigenvalue of $\tilde{W}(\lambda^*)$ for different scaling of the original graphs. Scaling down the measurements in the graph of Fig. 8(a) can re-establish the SZEP. Interestingly, this is in agreement with the convergence analysis of [10], which shows that the basin of convergence becomes larger when scaling down the inter-nodal distances.

7 Conclusion

We show that the application of Lagrangian duality in PGO provides an appealing approach to compute a globally optimal solution. More specifically, we propose four contributions. First, we rephrase PGO as a problem in complex variables. This allows drawing connection with the recent literature on *unit gain* graphs, and enables results on the spectrum of the pose graph matrix. Second, we formulate the Lagrangian dual problem and we analyze the relations between the primal and the dual solutions. Our key result proves that the duality gap is connected to the number of eigenvalues of the *penalized pose graph matrix*, which arises from the solution of the dual problem. In particular, if this matrix has a *single eigenvalue in zero* (SZEP), then (i) the duality gap is zero, (ii) the primal PGO problem has a unique solution (up to an arbitrary roto-translation), and (iii) the primal solution can be computed by *scaling* an eigenvector of the penalized pose graph matrix. The third contribution is an algorithm that returns a guaranteed optimal solution when the SZEP is satisfied, and (empirically) provides a very good estimate when the SZEP fails. Finally, we report numerical results, that show that (i) the SZEP holds for noise levels of practical robotics applications, (ii) the proposed algorithm outperforms several existing approaches, (iii) the satisfaction of the SZEP depends on multiple factors, including graph connectivity, number of poses, and measurement noise.

8 Appendix

8.1 Proof of Proposition 1: Zero Cost in Trees

We prove Proposition 1 by inspection, providing a procedure to build an estimate that annihilates every summand in (8). The procedure is as follows:

1. Select a root node, say the first node (p_i, r_i) , with $i = 1$, and set it to the origin, i.e., $p_i = 0_2$, $r_i = [1 \ 0]^\top$ (compare with (7) for $\theta_i = 0$);

2. For each neighbor j of the root i , if j is an outgoing neighbor, set $r_j = R_{ij}r_i$, and $p_j = p_i + D_{ij}r_i$, otherwise set $r_j = R_{ji}^\top r_i$, and $p_j = p_i + D_{ji}r_j$;
3. Repeat point 2 for the unknown neighbors of every node that has been computed so far, and continue until all poses have been computed.

Let us now show that this procedure produces a set of poses that annihilates the objective in (8). According to the procedure, we set the first node to the origin: $p_1 = 0_2$, $r_1 = [1 \ 0]^\top$; then, before moving to the second step of the procedure, we rearrange the terms in (8): we separate the edges into two sets $\mathcal{E} = \mathcal{E}_1 \cup \bar{\mathcal{E}}_1$, where \mathcal{E}_1 is the set of edges incident on node 1 (the root), and $\bar{\mathcal{E}}_1$ are the remaining edges. Then the cost can be written as:

$$\begin{aligned}
f(p, r) = & \sum_{(i,j) \in \mathcal{E}_1} \|p_j - p_i - D_{ij}r_i\|_2^2 + \|r_j - R_{ij}r_i\|_2^2 + \\
& + \sum_{(i,j) \in \bar{\mathcal{E}}_1} \|p_j - p_i - D_{ij}r_i\|_2^2 + \|r_j - R_{ij}r_i\|_2^2 \quad (48)
\end{aligned}$$

We can further split the set \mathcal{E}_1 into edges that have node 1 as a tail (i.e., edges in the form $(1, j)$) and edges that have node 1 as head (i.e., $(j, 1)$):

$$\begin{aligned}
f(p, r) = & \sum_{(1,j), j \in \mathcal{N}_1^{\text{out}}} \|p_j - p_1 - D_{1j}r_1\|_2^2 + \|r_j - R_{1j}r_1\|_2^2 + \\
& + \sum_{(j,1), j \in \mathcal{N}_1^{\text{in}}} \|p_1 - p_j - D_{j1}r_j\|_2^2 + \|r_1 - R_{j1}r_j\|_2^2 + \\
& + \sum_{(i,j) \in \bar{\mathcal{E}}_1} \|p_j - p_i - D_{ij}r_i\|_2^2 + \|r_j - R_{ij}r_i\|_2^2 \quad (49)
\end{aligned}$$

Now, we set each node j in the first two summands as prescribed in step 2 of the procedure. By inspection one can verify that this choice annihilates the first two summands and the cost becomes:

$$f(p, r) = \sum_{(i,j) \in \bar{\mathcal{E}}_1} \|p_j - p_i - D_{ij}r_i\|_2^2 + \|r_j - R_{ij}r_i\|_2^2 \quad (50)$$

Now we select a node k that has been computed at the previous step, but has some neighbor that is still unknown. As done previously, we split the set $\bar{\mathcal{E}}_1$ into two disjoint subsets: $\bar{\mathcal{E}}_1 = \mathcal{E}_k \cup \bar{\mathcal{E}}_k$, where the set \mathcal{E}_k contains the

edges in $\bar{\mathcal{E}}_1$ that are incident on k , and $\bar{\mathcal{E}}_k$ contains the remaining edges:

$$\begin{aligned}
f(p, r) = & \sum_{\{(k,j), j \in \mathcal{N}_k^{\text{out}}\} \cap \bar{\mathcal{E}}_1} \|p_j - p_k - D_{kj}r_k\|_2^2 + \|r_j - R_{kj}r_k\|_2^2 + \\
& + \sum_{\{(j,k), j \in \mathcal{N}_k^{\text{in}}\} \cap \bar{\mathcal{E}}_1} \|p_k - p_j - D_{jk}r_j\|_2^2 + \|r_k - R_{jk}r_j\|_2^2 + \\
& + \sum_{(i,j) \in \bar{\mathcal{E}}_k} \|p_j - p_i - D_{ij}r_i\|_2^2 + \|r_j - R_{ij}r_i\|_2^2 \quad (51)
\end{aligned}$$

Again, setting neighbors j as prescribed in step 2 of the procedure, annihilates the first two summands in (51). Repeating the same reasoning for all nodes that have been computed, but still have unknown neighbors, we can easily show that all terms in (51) become zero (the assumption of graph connectivity ensures that we can reach all nodes), proving the claim.

8.2 Proof of Proposition 2: Zero Cost in Balanced Graphs

Similarly to Appendix 8.1, we prove Proposition 2 by showing that in balanced graphs one can always build a solution that attains zero cost.

For the assumption of connectivity, we can find a spanning tree \mathcal{T} of the graph, and split the terms in the cost function accordingly:

$$\begin{aligned}
f(p, r) = & \sum_{(i,j) \in \mathcal{T}} \|p_j - p_i - D_{ij}r_i\|_2^2 + \|r_j - R_{ij}r_i\|_2^2 + \\
& + \sum_{(i,j) \in \bar{\mathcal{T}}} \|p_j - p_i - D_{ij}r_i\|_2^2 + \|r_j - R_{ij}r_i\|_2^2 \quad (52)
\end{aligned}$$

where $\bar{\mathcal{T}} \doteq \mathcal{E} \setminus \mathcal{T}$ are the *chords* of the graph w.r.t. \mathcal{T} .

Then, using the procedure in Appendix 8.1 we construct a solution $\{r_i^*, p_i^*\}$ that attains zero cost for the measurements in the spanning tree \mathcal{T} . Therefore, our claim only requires to demonstrate that the solution built from the spanning tree also annihilates the terms in $\bar{\mathcal{T}}$:

$$f(p^*, r^*) = \sum_{(i,j) \in \bar{\mathcal{T}}} \|p_j^* - p_i^* - D_{ij}r_i^*\|_2^2 + \|r_j^* - R_{ij}r_i^*\|_2^2 \quad (53)$$

To prove the claim, we consider one of the chords in $\bar{\mathcal{T}}$ and we show that the cost at $\{r_i^*, p_i^*\}$ is zero. The cost associated to a chord $(i, j) \in \bar{\mathcal{T}}$ is:

$$\|p_j^* - p_i^* - D_{ij}r_i^*\|_2^2 + \|r_j^* - R_{ij}r_i^*\|_2^2 \quad (54)$$

Now consider the unique path \mathcal{P}_{ij} in the spanning tree \mathcal{T} that connects i to j , and number the nodes along this path as $i, i+1, \dots, j-1, j$.

Let us start by analyzing the second summand in (54), which corresponds to the rotation measurements. According to the procedure in Appendix 8.1 to build the solution for \mathcal{T} , we propagate the estimate from the root of the tree. Then it is easy to see that:

$$r_j^* = R_{j-1j} \cdots R_{i+1i+2} R_{ii+1} r_i^* \quad (55)$$

where R_{ii+1} is the rotation associated to the edge $(i, i+1)$, or its transpose if the edge is in the form $(i+1, i)$ (i.e., it is traversed backwards along \mathcal{P}_{ij}). Now we notice that the assumption of balanced graph implies that the measurements compose to the identity along every cycle in the graph. Since the chord (i, j) and the path \mathcal{P}_{ij} form a cycle in the graph, it holds:

$$R_{j-1j} \cdots R_{i+1i+2} R_{ii+1} = R_{ij} \quad (56)$$

Substituting (56) back into (55) we get:

$$r_j^* = R_{ij} r_i^* \quad (57)$$

which can be easily seen to annihilate the second summand in (54).

Now we only need to demonstrate that also the first summand in (54) is zero. The procedure in Appendix 8.1 leads to the following estimate for the position of node j :

$$\begin{aligned} p_j^* &= p_i^* + D_{ii+1} r_i^* + D_{i+1i+2} r_{i+1}^* + \cdots + D_{j-1j} r_{j-1}^* \quad (58) \\ &= p_i^* + D_{ii+1} r_i^* + D_{i+1i+2} R_{ii+1} r_i^* + \cdots + D_{j-1j} R_{j-2j-1} \cdots R_{i+1i+2} R_{ii+1} r_i^* \\ &= p_i^* + (D_{ii+1} + D_{i+1i+2} R_{ii+1} + \cdots + D_{j-1j} R_{j-2j-1} \cdots R_{i+1i+2} R_{ii+1}) r_i^* \end{aligned}$$

The assumption of balanced graph implies that position measurements compose to zero along every cycle, hence:

$$\begin{aligned} \Delta_{ij} &= \Delta_{ii+1} + R_{ii+1} \Delta_{i+1i+2} + R_{i+1i+2} R_{ii+1} \Delta_{i+2i+3} + \cdots \\ &\quad + R_{j-2j-1} \cdots R_{i+1i+2} R_{ii+1} \Delta_{j-1j} \end{aligned} \quad (59)$$

or equivalently:

$$\begin{aligned} D_{ij} &= D_{ii+1} + D_{i+1i+2} R_{ii+1} + \cdots \\ &\quad + D_{j-1j} R_{j-2j-1} \cdots R_{i+1i+2} R_{ii+1} \end{aligned} \quad (60)$$

Substituting (60) back into (58) we obtain:

$$p_j^* = p_i^* + D_{ij} r_i^*$$

which annihilates the first summand in (54), concluding the proof.

8.3 Proof of Proposition 4: properties of \mathcal{W}

Let us prove that \mathcal{W} has (at least) two eigenvalues in zero. We already observed that the top-left block of \mathcal{W} is $\bar{\mathcal{L}} = \mathcal{L} \otimes I_2$, where \mathcal{L} is the Laplacian matrix of the graph underlying the PGO problem. The Laplacian \mathcal{L} of a connected graph has a single eigenvalue in zero, and the corresponding eigenvector is $\mathbf{1}_n$ (see, e.g., [18, Sections 1.2-1.3]), i.e., $\mathcal{L} \cdot \mathbf{1}_n = 0$. Using this property, it is easy to show that the matrix $N \doteq [0_n^\top \ \mathbf{1}_n^\top]^\top \otimes I_2$ is in the nullspace of \mathcal{W} , i.e., $\mathcal{W}N = 0$. Since N has rank 2, this implies that the nullspace of \mathcal{W} has at least dimension 2, which proves the first claim.

Let us now prove that the matrix \mathcal{W} is composed by 2×2 blocks $[\mathcal{W}]_{ij}$, with $[\mathcal{W}]_{ij} \in \alpha SO(2)$, $\forall i, j = 1, \dots, 2n$, and $[\mathcal{W}]_{ii} = \alpha_{ii} I_2$ with $\alpha_{ii} \geq 0$. We prove this by direct inspection of the blocks of \mathcal{W} . Given the structure of \mathcal{W} in (14), the claim reduces to proving that the matrices $\bar{\mathcal{L}}$, \bar{Q} , and $\bar{A}^\top \bar{D}$ are composed by 2×2 blocks in $\alpha SO(2)$, and the diagonal blocks of $\bar{\mathcal{L}}$ and \bar{Q} are multiples of the identity matrix. To this end, we start by observing that $\bar{\mathcal{L}} = \mathcal{L} \otimes I_2$, hence all blocks in $\bar{\mathcal{L}}$ are multiples of the 2×2 identity matrix, which also implies that they belong to $\alpha SO(2)$. Consider next the matrix $\bar{Q} \doteq \bar{D}^\top \bar{D} + \bar{U}^\top \bar{U}$. From the definition of \bar{D} it follows that $\bar{D}^\top \bar{D}$ is zero everywhere, except the 2×2 diagonal blocks:

$$[\bar{D}^\top \bar{D}]_{ii} = \sum_{j \in \mathcal{N}_i^{\text{out}}} \|\Delta_{ij}\|_2^2 I_2, \quad i = 1, \dots, n. \quad (61)$$

Similarly, from simple matrix manipulation we obtain the following block structure of $\bar{U}^\top \bar{U}$:

$$\begin{aligned} [\bar{U}^\top \bar{U}]_{ii} &= d_i I_2, & i = 1, \dots, n; \\ [\bar{U}^\top \bar{U}]_{ij} &= -R_{ij}, & (i, j) \in \mathcal{E}; \\ [\bar{U}^\top \bar{U}]_{ij} &= -R_{ji}^\top, & (j, i) \in \mathcal{E}; \\ [\bar{U}^\top \bar{U}]_{ij} &= 0_{2 \times 2}, & \text{otherwise.} \end{aligned} \quad (62)$$

where d_i is the degree (number of neighbours) of node i . Combining (61) and (62) we get the following structure for \bar{Q} :

$$\begin{aligned} [\bar{Q}]_{ii} &= \beta_i I_2, & i = 1, \dots, n; \\ [\bar{Q}]_{ij} &= -R_{ij}, & (i, j) \in \mathcal{E}; \\ [\bar{Q}]_{ij} &= -R_{ji}^\top, & (j, i) \in \mathcal{E}; \\ [\bar{Q}]_{ij} &= 0_{2 \times 2}, & \text{otherwise.} \end{aligned} \quad (63)$$

where we defined $\beta_i \doteq d_i + \sum_{j \in \mathcal{N}_i^{\text{out}}} \|\Delta_{ij}\|_2^2$. Clearly, \bar{Q} has blocks in $\alpha SO(2)$ and the diagonal blocks are nonnegative multiples of I_2 .

Now, it only remains to inspect the structure of $\bar{A}^\top \bar{D}$. The matrix $\bar{A}^\top \bar{D}$ has the following structure:

$$\begin{aligned} [\bar{A}^\top \bar{D}]_{ii} &= \sum_{j \in \mathcal{N}_i^{\text{out}}} D_{ij}, & i = 1, \dots, n; \\ [\bar{A}^\top \bar{D}]_{ij} &= -D_{ji}, & (j, i) \in \mathcal{E}; \\ [\bar{A}^\top \bar{D}]_{ij} &= 0_{2 \times 2}, & \text{otherwise.} \end{aligned} \quad (64)$$

Note that $\sum_{j \in \mathcal{N}_i^{\text{out}}} D_{ij}$ is the sum of matrices in $\alpha SO(2)$, hence it also belongs to $\alpha SO(2)$. Therefore, also all blocks of $\bar{A}^\top \bar{D}$ are in $\alpha SO(2)$, thus concluding the proof.

8.4 Proof of Proposition 5: Cost in the Complex Domain

Let us prove the equivalence between the complex cost and its real counterpart, as stated in Proposition 5.

We first observe that the dot product between two 2-vectors $x_1, x_2 \in \mathbb{R}^2$, can be written in terms of their complex representation $\tilde{x}_1 \doteq x_1^\vee$, and $\tilde{x}_2 \doteq x_2^\vee$, as follows:

$$x_1^\top x_2 = \frac{\tilde{x}_1^* \tilde{x}_2 + \tilde{x}_1 \tilde{x}_2^*}{2} \quad (65)$$

Moreover, we know that the action of a matrix $Z \in \alpha SO(2)$ can be written as the product of complex numbers, see (18).

Combining (65) and (18) we get:

$$x_1^\top Z x_2 \sim \frac{\tilde{x}_1^* \tilde{z} \tilde{x}_2 + \tilde{x}_1 \tilde{z}^* \tilde{x}_2^*}{2} \quad (66)$$

where $\tilde{z} = Z^\vee$. Furthermore, when Z is multiple of the identity matrix, it is easy to see that $z = Z^\vee$ is actually a real number, and Eq. (66) becomes:

$$x_1^\top Z x_1 \sim \tilde{x}_1^* z \tilde{x}_1 \quad (67)$$

With the machinery introduced so far, we are ready to rewrite the cost $x^\top W x$ in complex form. Since W is symmetric, the product becomes:

$$x^\top W x = \sum_{i=1}^{2n-1} \left[x_i^\top [W]_{ii} x_i + \sum_{j=i+1}^{2n-1} 2 x_i^\top [W]_{ij} x_j \right] \quad (68)$$

Using the fact that $[W]_{ii}$ is a multiple of the identity matrix, $\tilde{W}_{ii} \doteq [W]_{ii}^\vee \in \mathbb{R}$, and using (67) we conclude $x_i^\top [W]_{ii} x_i = \tilde{x}_i^* \tilde{W}_{ii} \tilde{x}_i$. Moreover, defining $\tilde{W}_{ij} \doteq [W]_{ij}^\vee$ (these will be complex numbers, in general), and using (66), eq. (68) becomes:

$$\begin{aligned} x^\top W x &= \sum_{i=1}^{2n-1} \left[\tilde{x}_i^* \tilde{W}_{ii} \tilde{x}_i + \sum_{j=i+1}^{2n-1} (\tilde{x}_i^* \tilde{W}_{ij} \tilde{x}_j + \tilde{x}_i \tilde{W}_{ij}^* \tilde{x}_j^*) \right] \\ &= \sum_{i=1}^{2n-1} \left[\tilde{x}_i^* \tilde{W}_{ii} \tilde{x}_i + \sum_{j \neq i} \tilde{x}_i^* \tilde{W}_{ij} \tilde{x}_j \right] = \tilde{x}^* \tilde{W} \tilde{x} \end{aligned} \quad (69)$$

where we completed the lower triangular part of \tilde{W} as $\tilde{W}_{ji} = \tilde{W}_{ij}^*$.

8.5 Proof of Proposition 6: Zero Eigenvalues in \tilde{W}

Let us denote with N_0 the number of zero eigenvalues of the pose graph matrix \tilde{W} . N_0 can be written in terms of the dimension of the matrix ($\tilde{W} \in \mathbb{C}^{(2n-1) \times (2n-1)}$) and the rank of the matrix:

$$N_0 = (2n - 1) - \text{rank}(\tilde{W}) \quad (70)$$

Now, recalling the factorization of \tilde{W} given in (25), we note that:

$$\text{rank}(\tilde{W}) = \text{rank} \left(\begin{bmatrix} A & \tilde{D} \\ 0 & \tilde{U} \end{bmatrix} \right) = \text{rank}(A) + \text{rank}(\tilde{U}) \quad (71)$$

where the second relation follows from the upper triangular structure of the matrix. Now, we know from [67, Section 19.3] that the anchored incidence matrix A , obtained by removing a row from the the incidence matrix of a connected graph, is full rank:

$$\text{rank}(A) = n - 1 \quad (72)$$

Therefore:

$$N_0 = n - \text{rank}(\tilde{U}) \quad (73)$$

Now, since we recognized that \tilde{U} is the complex incidence matrix of a unit gain graph (Lemma 1), we can use the result of Lemma 2.3 in [60], which says that:

$$\text{rank}(\tilde{U}) = n - b, \quad (74)$$

where b is the number of connected components in the graph that are balanced. Since we are working on a connected graph (Assumption 1), b can be

either one (balanced graph or tree), or zero otherwise. Using (73) and (74), we obtain $N_0 = b$, which implies that that $N_0 = 1$ for balanced graphs or trees, or $N_0 = 0$, otherwise.

8.6 Proof of Proposition 7: Spectrum of Complex and Real Pose Graph Matrices

Recall that any Hermitian matrix has real eigenvalues, and possibly complex eigenvectors. Let $\mu \in \mathbb{R}$ be an eigenvalue of \tilde{W} , associated with an eigenvector $\tilde{v} \in \mathbb{C}^{2n-1}$, i.e.,

$$\tilde{W}\tilde{v} = \mu\tilde{v} \quad (75)$$

From equation (75) we have, for $i = 1, \dots, 2n - 1$,

$$\sum_{j=1}^{2n-1} \tilde{W}_{ij}\tilde{v}_j = \mu\tilde{v}_i \Leftrightarrow \sum_{j=1}^{2n-1} [W]_{ij}v_j = \mu v_i \quad (76)$$

where v_i is such that $v_i^\vee = \tilde{v}_i$. Since eq. (76) holds for all $i = 1, \dots, 2n - 1$, it can be written in compact form as:

$$Wv = \mu v \quad (77)$$

hence v is an eigenvector of the real anchored pose graph matrix W , associated with the eigenvalue μ . This proves that any eigenvalue of \tilde{W} is also an eigenvalue of W .

To prove that the eigenvalue μ is actually repeated twice in W , consider now equation (75) and multiply both members by the complex number $e^{j\frac{\pi}{2}}$:

$$\tilde{W}\tilde{v}e^{j\frac{\pi}{2}} = \mu\tilde{v}e^{j\frac{\pi}{2}} \quad (78)$$

For $i = 1, \dots, 2n - 1$, we have:

$$\sum_{j=1}^{2n-1} \tilde{W}_{ij}^*\tilde{v}_je^{j\frac{\pi}{2}} = \mu\tilde{v}_ie^{j\frac{\pi}{2}} \Leftrightarrow \sum_{j=1}^{2n-1} [W]_{ij}w_j = \mu w_i \quad (79)$$

where w_i is such that $w_i^\vee = \tilde{v}_ie^{j\frac{\pi}{2}}$. Since eq. (79) holds for all $i = 1, \dots, 2n - 1$, it can be written in compact form as:

$$Ww = \mu w \quad (80)$$

hence also w is an eigenvector of W associated with the eigenvalue μ .

Now it only remains to demonstrate that v and w are linearly independent. One can readily check that, if \tilde{v}_i is in the form $\tilde{v}_i = \eta_i e^{j\theta_i}$, then

$$v_i = \eta_i \begin{bmatrix} \cos(\theta_i) \\ \sin(\theta_i) \end{bmatrix}. \quad (81)$$

Moreover, observing that $\tilde{v}_j e^{j\frac{\pi}{2}} = \eta_j e^{j(\theta_j + \pi/2)}$, then

$$w_i = \eta_i \begin{bmatrix} \cos(\theta_i + \pi/2) \\ \sin(\theta_i + \pi/2) \end{bmatrix} = \eta_i \begin{bmatrix} -\sin(\theta_i) \\ \cos(\theta_i) \end{bmatrix} \quad (82)$$

From (81) and (82) it is easy to see that $v^\top w = 0$, thus v, w are orthogonal, hence independent. To each eigenvalue μ of \tilde{W} there thus correspond an identical eigenvalue of W , of geometric multiplicity at least two. Since \tilde{W} has $2n - 1$ eigenvalues and W has $2(2n - 1)$ eigenvalues, we conclude that to each eigenvalue μ of \tilde{W} there correspond exactly two eigenvalues of W in μ . The previous proof also shows how the set of orthogonal eigenvectors of W is related to the set of eigenvectors of \tilde{W} .

8.7 Proof of Theorem 1: Primal-dual Optimal Pairs

We prove that, given $\lambda \in \mathbb{R}^n$, if an $\tilde{x}_\lambda \in \mathcal{X}(\lambda)$ is primal feasible, then \tilde{x}_λ is primal optimal; moreover, λ is dual optimal, and the duality gap is zero.

By weak duality we know that for any λ :

$$\mathcal{L}(x_\lambda, \lambda) \leq f^* \quad (83)$$

However, if x_λ is primal feasible, by optimality of f^* , it must also hold

$$f^* \leq f(x_\lambda) \quad (84)$$

Now we observe that for a feasible x_λ , the terms in the Lagrangian associated to the constraints disappear and $\mathcal{L}(x_\lambda, \lambda) = f(x_\lambda)$. Using the latter equality and the inequalities (83) and (84) we get:

$$f^* \leq f(x_\lambda) = \mathcal{L}(x_\lambda, \lambda) \leq f^* \quad (85)$$

which implies $f(x_\lambda) = f^*$, i.e., x_λ is primal optimal.

Further, we have that

$$d^* \geq \min_x \mathcal{L}(x, \lambda) = \mathcal{L}(x_\lambda, \lambda) = f(x_\lambda) = f^*,$$

which, combined with weak duality ($d^* \leq f^*$), implies that $d^* = f^*$ and that λ attains the dual optimal value.

8.8 Numerical Data For the Toy Examples in Section 6

Ground truth nodes poses, written as $x_i = [p_i^\top, \theta_i]$:

$$\begin{aligned}
 x_1 &= [0.0000 & -5.0000 & 0.2451] \\
 x_2 &= [4.7553 & -1.5451 & -0.4496] \\
 x_3 &= [2.9389 & 4.0451 & 0.7361] \\
 x_4 &= [-2.9389 & 4.0451 & 0.3699] \\
 x_5 &= [-4.7553 & -1.5451 & -1.7225]
 \end{aligned} \tag{86}$$

Relative measurements, for each edge (i, j) , written as $(i, j) : [\Delta ij^\top, \theta_{ij}]$:

$$\begin{aligned}
 (1, 2) &: [4.6606 & 1.2177 & 2.8186] \\
 (2, 3) &: [-4.4199 & 4.8043 & 0.1519] \\
 (3, 4) &: [-4.1169 & 4.9322 & 0.5638] \\
 (4, 5) &: [-3.6351 & -5.0908 & -0.5855] \\
 (5, 1) &: [3.4744 & 5.9425 & 2.5775]
 \end{aligned} \tag{87}$$

References

- [1] R. Aragues, L. Carlone, G. Calafiore, and C. Sagues. Multi-agent localization from noisy relative pose measurements. In *IEEE Intl. Conf. on Robotics and Automation (ICRA)*, pages 364–369, Shanghai, China, 2011.
- [2] M. Arie-Nachimson, S. Z. Kovalsky, I. Kemelmacher-Shlizerman, A. Singer, and R. Basri. Global motion estimation from point matches. In *3DIMPVT*, 2012.
- [3] A.S. Bandeira, A. Singer, and D.A. Spielman. A Cheeger inequality for the graph connection laplacian. *SIAM. J. Matrix Anal. & Appl.*, 34(4):1611–1630, 2013.
- [4] P. Barooah and J.P. Hespanha. Estimation on graphs from relative measurements. *Control System Magazine*, 27(4):57–74, 2007.
- [5] P. Biswas, T. Lian, T. Wang, and Y. Ye. Semidefinite programming based algorithms for sensor network localization. *ACM Transactions on Sensor Networks*, 2(2):188–220, 2006.
- [6] D. Borra, R. Carli, E. Lovisari, F. Fagnani, and S. Zampieri. Autonomous calibration algorithms for planar networks of cameras. *Automatica*, 2012.

- [7] S. Boyd and L. Vandenberghe. *Convex optimization*. Cambridge University Press, 2004.
- [8] G.C. Calafiore, L. Carlone, and M. Wei. Distributed optimization techniques for range localization in networked systems. In *IEEE Conf. on Decision and Control*, pages 2221–2226, 2010.
- [9] Nicholas Carlevaris-Bianco and Ryan M. Eustice. Generic factor-based node marginalization and edge sparsification for pose-graph SLAM. In *IEEE Intl. Conf. on Robotics and Automation (ICRA)*, pages 5728–5735, 2013.
- [10] L. Carlone. Convergence analysis of pose graph optimization via Gauss-Newton methods. In *IEEE Intl. Conf. on Robotics and Automation (ICRA)*, pages 965–972, 2013.
- [11] L. Carlone, R. Aragues, J.A. Castellanos, and B. Bona. A linear approximation for graph-based simultaneous localization and mapping. In *Robotics: Science and Systems (RSS)*, 2011.
- [12] L. Carlone, R. Aragues, J.A. Castellanos, and B. Bona. A fast and accurate approximation for planar pose graph optimization. *Intl. J. of Robotics Research*, 2014.
- [13] L. Carlone and A. Censi. From angular manifolds to the integer lattice: Guaranteed orientation estimation with application to pose graph optimization. *IEEE Trans. Robotics*, 2014.
- [14] L. Carlone and F. Dellaert. Duality-based verification techniques for 2D SLAM. In *Intl. Conf. on Robotics and Automation (ICRA)*, *accepted*, 2015.
- [15] L. Carlone, R. Tron, K. Daniilidis, and F. Dellaert. Initialization techniques for 3D SLAM: a survey on rotation estimation and its use in pose graph optimization. In *IEEE Intl. Conf. on Robotics and Automation (ICRA)*, 2015.
- [16] G. S. Chirikjian. *Stochastic Models, Information Theory, and Lie Groups, Volume 2: Analytic Methods and Modern Applications (Applied and Numerical Harmonic Analysis)*. Birkhauser, 2012.
- [17] A. Chiuso, G. Picci, and S. Soatto. Wide-sense estimation on the special orthogonal group. *Commun. Inf. Syst.*, 8:185–200, 2008.

- [18] F.R.K. Chung. *Spectral Graph Theory*. American Mathematical Soc., CBMS Regional Conference Series in Mathematics, No. 92, 1996.
- [19] J. Costa, N. Patwari, and A. Hero. Distributed weighted-multidimensional scaling for node localization in sensor networks. *ACM Transactions on Sensor Networks*, 2(1):39–64, 2006.
- [20] M. Cucuringu, Y. Lipman, and A. Singer. Sensor network localization by eigenvector synchronization over the euclidean group. *ACM Transactions on Sensor Networks*, 8(3):19:1–19:42, 2012.
- [21] M. Cucuringu, A. Singer, and D. Cowburn. Eigenvector synchronization, graph rigidity and the molecule problem. *Information and Inference: A Journal of the IMA*, 1(1):21–67, 2012.
- [22] F. Dellaert, J. Carlson, V. Ila, K. Ni, and C.E. Thorpe. Subgraph-preconditioned conjugate gradient for large scale slam. In *IEEE/RSJ Intl. Conf. on Intelligent Robots and Systems (IROS)*, 2010.
- [23] L. Doherty, K. Pister, and L. El Ghaoui. Convex position estimation in wireless sensor networks. In *IEEE INFOCOM, Volume 3*, pages 1655–1663, 2001.
- [24] G. Dubbelman and B. Browning. Closed-form online pose-chain slam. In *IEEE Intl. Conf. on Robotics and Automation (ICRA)*, 2013.
- [25] G. Dubbelman, I. Esteban, and K. Schutte. Efficient trajectory bending with applications to loop closure. In *IEEE/RSJ Intl. Conf. on Intelligent Robots and Systems (IROS)*, pages 1–7, 2010.
- [26] G. Dubbelman, P. Hansen, B. Browning, and M.B. Dias. Orientation only loop-closing with closed-form trajectory bending. In *IEEE Intl. Conf. on Robotics and Automation (ICRA)*, 2012.
- [27] T. Duckett, S. Marsland, and J. Shapiro. Fast, on-line learning of globally consistent maps. *Autonomous Robots*, 12(3):287–300, 2002.
- [28] C. Eckart and G. Young. The approximation of one matrix by another low rank. *Psychometrika*, 1:211–218, 1936.
- [29] M. Hazewinkel ed. *Complex number, Encyclopedia of Mathematics*. Springer, 2001.

- [30] T. Eren, O.K. Goldenberg, W. Whiteley, and Y.R. Yang. Rigidity, computation, and randomization in network localization. In *INFOCOM 2004. Twenty-third Annual Joint Conference of the IEEE Computer and Communications Societies, Volume:4*, pages 2673–2684. IEEE, 2004.
- [31] T. Eren, W. Whiteley, and P.N. Belhumeur. Using angle of arrival (bearing) information in network localization. In *IEEE Conf. on Decision and Control*, pages 4676–4681, 2006.
- [32] R.M. Eustice, H. Singh, J.J. Leonard, and M.R. Walter. Visually mapping the RMS Titanic: Conservative covariance estimates for SLAM information filters. *Intl. J. of Robotics Research*, 25(12):1223–1242, Dec 2006.
- [33] J. Fredriksson and C. Olsson. Simultaneous multiple rotation averaging using lagrangian duality. In *Asian Conf. on Computer Vision (ACCV)*, 2012.
- [34] U. Frese, P. Larsson, and T. Duckett. A multilevel relaxation algorithm for simultaneous localisation and mapping. *IEEE Trans. Robotics*, 21(2):196–207, April 2005.
- [35] V. M. Govindu. Combining two-view constraints for motion estimation. In *IEEE Conf. on Computer Vision and Pattern Recognition (CVPR)*, pages 218–225, 2001.
- [36] V.M. Govindu. Lie-algebraic averaging for globally consistent motion estimation. In *IEEE Conf. on Computer Vision and Pattern Recognition (CVPR)*, 2004.
- [37] G. Grisetti, C. Stachniss, and W. Burgard. Non-linear constraint network optimization for efficient map learning. *Trans. on Intelligent Transportation systems*, 10(3):428–439, 2009.
- [38] R. Hartley, J. Trumpf, Y. Dai, and H. Li. Rotation averaging. *IJCV*, 103(3):267–305, 2013.
- [39] T. Hatanaka, M. Fujita, and F. Bullo. Vision-based cooperative estimation via multi-agent optimization. In *IEEE Conf. on Decision and Control*, 2010.
- [40] S. Huang, Y. Lai, U. Frese, and G. Dissanayake. How far is SLAM from a linear least squares problem? In *IEEE/RSJ Intl. Conf. on Intelligent Robots and Systems (IROS)*, pages 3011–3016, 2010.

- [41] S. Huang, H. Wang, U. Frese, and G. Dissanayake. On the number of local minima to the point feature based SLAM problem. In *IEEE Intl. Conf. on Robotics and Automation (ICRA)*, pages 2074–2079, 2012.
- [42] V. Indelman, E. Nelson, N. Michael, and F. Dellaert. Multi-robot pose graph localization and data association from unknown initial relative poses via expectation maximization. In *IEEE Intl. Conf. on Robotics and Automation (ICRA)*, 2014.
- [43] H. Johannsson, M. Kaess, M. Fallon, and J.J. Leonard. Temporally scalable visual SLAM using a reduced pose graph. In *IEEE Intl. Conf. on Robotics and Automation (ICRA)*, pages 54–61, 2013.
- [44] M. Kaess, H. Johannsson, R. Roberts, V. Ila, J. Leonard, and F. Dellaert. iSAM2: Incremental smoothing and mapping using the Bayes tree. *Intl. J. of Robotics Research*, 31:217–236, Feb 2012.
- [45] M. Kaess, A. Ranganathan, and F. Dellaert. iSAM: Incremental smoothing and mapping. *IEEE Trans. Robotics*, 24(6):1365–1378, Dec 2008.
- [46] B. Kim, M. Kaess, L. Fletcher, J. Leonard, A. Bachrach, N. Roy, and S. Teller. Multiple relative pose graphs for robust cooperative mapping. In *IEEE Intl. Conf. on Robotics and Automation (ICRA)*, pages 3185–3192, Anchorage, Alaska, May 2010.
- [47] J. Knuth and P. Barooah. Collaborative 3D localization of robots from relative pose measurements using gradient descent on manifolds. In *IEEE Intl. Conf. on Robotics and Automation (ICRA)*, pages 1101–1106, 2012.
- [48] J. Knuth and P. Barooah. Collaborative localization with heterogeneous inter-robot measurements by Riemannian optimization. In *IEEE Intl. Conf. on Robotics and Automation (ICRA)*, 2013.
- [49] J. Knuth and P. Barooah. Error growth in position estimation from noisy relative pose measurements. *Robotics and Autonomous Systems*, 61(3):229–224, 2013.
- [50] K. Konolige. Large-scale map-making. In *Proc. 21th AAAI National Conference on AI*, San Jose, CA, 2004.

- [51] R. Kümmerle, G. Grisetti, H. Strasdat, K. Konolige, and W. Burgard. g2o: A general framework for graph optimization. In *Proc. of the IEEE Int. Conf. on Robotics and Automation (ICRA)*, Shanghai, China, May 2011.
- [52] K. Levenberg. A method for the solution of certain nonlinear problems in least squares. *Quart. Appl. Math*, 2(2):164–168, 1944.
- [53] F. Lu and E. Milios. Globally consistent range scan alignment for environment mapping. *Autonomous Robots*, pages 333–349, Apr 1997.
- [54] G. Mao, B. Fidan, and B. Anderson. Wireless sensor network localization techniques. *Computer Networks*, 51(10):2529–2553, 2007.
- [55] D. Martinec and T. Pajdla. Robust rotation and translation estimation in multiview reconstruction. In *IEEE Conf. on Computer Vision and Pattern Recognition (CVPR)*, pages 1–8, 2007.
- [56] R. Olfati-Saber. Swarms on sphere: A programmable swarm with synchronous behaviors like oscillator networks. In *IEEE Conf. on Decision and Control*, pages 5060–5066, 2006.
- [57] E. Olson, J. Leonard, and S. Teller. Fast iterative alignment of pose graphs with poor initial estimates. In *IEEE Intl. Conf. on Robotics and Automation (ICRA)*, pages 2262–2269, May 2006.
- [58] J. R. Peters, D. Borra, B. Paden, and F. Bullo. Sensor network localization on the group of 3D displacements. *SIAM Journal on Control and Optimization*, submitted, 2014.
- [59] G. Piovan, I. Shames, B. Fidan, F. Bullo, and B. Anderson. On frame and orientation localization for relative sensing networks. *Automatica*, 49(1):206–213, 2013.
- [60] N. Reff. Spectral properties of complex unit graphs. *arXiv*, 2011.
- [61] D.M. Rosen, M. Kaess, and J.J. Leonard. An incremental trust-region method for robust online sparse least-squares estimation. In *IEEE Intl. Conf. on Robotics and Automation (ICRA)*, pages 1262–1269, St. Paul, MN, May 2012.
- [62] D.M. Rosen, M. Kaess, and J.J. Leonard. RISE: An incremental trust-region method for robust online sparse least-squares estimation. *IEEE Trans. Robotics*, 2014.

- [63] W.J. Russell, D.J. Klein, and J.P. Hespanha. Optimal estimation on the graph cycle space. *59(6):2834–2846*, 2011.
- [64] A. Sarlette and R. Sepulchre. Consensus optimization on manifolds. *SIAM J. Control and Optimization*, 48(1):56–76, 2009.
- [65] J. Saunderson, P.A. Parrilo, and A. Willsky. Semidefinite descriptions of the convex hull of rotation matrices. *ArXiv preprint: <http://arxiv.org/abs/1403.4914>*, 2014.
- [66] J. Saunderson, P.A. Parrilo, and A. Willsky. Semidefinite relaxations for optimization problems over rotation matrices. In *IEEE Conf. on Decision and Control*, May 2014.
- [67] Al. Schrijver. *Theory of Linear and Integer Programming*. Wiley, 1998.
- [68] G.C. Sharp, S.W. Lee, and D.K. Wehe. Multiview registration of 3D scenes by minimizing error between coordinate frames. *IEEE Trans. Pattern Anal. Machine Intell.*, 26(8):1037–1050, 2004.
- [69] A. Singer. A remark on global positioning from local distances. *Proceedings of the National Academy of Sciences*, 105(28):9507–9511, 2008.
- [70] A. Singer. Angular synchronization by eigenvectors and semidefinite programming. *Appl. Comput. Harmon. Anal.*, 30:20–36, 2010.
- [71] A. Singer and Y. Shkolnisky. Three-dimensional structure determination from common lines in Cryo-EM by eigenvectors and semidefinite programming. *SIAM J. Imaging Sciences*, pages 543–572, 2011.
- [72] R. Stanfield. Statistical theory of DF finding. *Journal of IEE*, 94(5):762–770, 1947.
- [73] J. Thunberg, E. Montijano, and X. Hu. Distributed attitude synchronization control. In *IEEE Conf. on Decision and Control*, 2011.
- [74] R. Tron, B. Afsari, and R. Vidal. Intrinsic consensus on $SO(3)$ with almost global convergence. In *IEEE Conf. on Decision and Control*, 2012.
- [75] R. Tron, B. Afsari, and R. Vidal. Riemannian consensus for manifolds with bounded curvature. *IEEE Trans. on Automatic Control*, 2012.

- [76] R. Tron, L. Carlone, F. Dellaert, and K. Daniilidis. Rigid components identification and rigidity enforcement in bearing-only localization using the graph cycle basis. In *American Control Conference*, 2015.
- [77] R. Tron and R. Vidal. Distributed image-based 3-D localization in camera networks. In *IEEE Conf. on Decision and Control*, 2009.
- [78] H. Wang, G. Hu, S. Huang, and G. Dissanayake. On the structure of nonlinearities in pose graph SLAM. In *Robotics: Science and Systems (RSS)*, 2012.
- [79] L. Wang and A. Singer. Exact and stable recovery of rotations for robust synchronization. *Information and Inference: A Journal of the IMA*, 30, 2013.
- [80] S. Zhang. Quadratic maximization and semidefinite relaxation. *Math. Programming, Ser. A*, 87:453–465, 2000.